The nucleolus functions as a phase-separated protein quality control compartment

Authors: F. Frottin[1], F. Schueder[2,3], S. Tiwary[4], R. Gupta[1*], R. Körner[1], T. Schlichthaerle[2,3], J. Cox[4], R. Jungmann[2,3§], F.U. Hartl[1,5§], M.S. Hipp[1,5§]

Affiliations:

[1] Department of Cellular Biochemistry, Max Planck Institute of Biochemistry, D-82152 Martinsried, Germany.

[2] Research Group "Molecular Imaging and Bionanotechnology", Max Planck Institute of Biochemistry, D-82152 Martinsried, Germany.

[3] Faculty of Physics and Center for Nanoscience, Ludwig Maximilian University, D-80539 Munich, Germany.

[4] Research Group "Computational Systems Biochemistry", Max Planck Institute of Biochemistry, D-82152 Martinsried, Germany.

[5] Munich Cluster for Systems Neurology (SyNergy), D-80336 Munich, Germany.

§ Correspondence to: uhartl@biochem.mpg.de (F.U.H.); hipp@biochem.mpg.de (M.S.H.); jungmann@biochem.mpg.de (R.J.)

* present address: The Novo Nordisk Foundation Center for Protein Research, Faculty of Health and Medical Sciences, University of Copenhagen, DK-2200 Copenhagen, Denmark.

Abstract: The nuclear proteome is rich in stress-sensitive proteins, suggesting that effective protein quality control mechanisms are in place to ensure conformational maintenance. Here we investigated the role of the nucleolus in this process. In mammalian tissue culture cells, under stress conditions misfolded proteins entered the granular component (GC) phase of the nucleolus. Transient associations with nucleolar proteins such as NPM1 conferred low mobility to misfolded proteins within the liquid-like GC phase, avoiding irreversible aggregation. Refolding and extraction of proteins from the nucleolus during recovery from stress was Hsp70 dependent. The capacity of the nucleolus to store misfolded proteins was limited and prolonged stress led to a transition of the nucleolar matrix from liquid-like to solid, with loss of reversibility and dysfunction in quality control. Thus we suggest that the nucleolus has chaperone-like properties and can promote nuclear protein maintenance under stress.

One Sentence Summary: The liquid-like nucleolar compartment prevents irreversible protein aggregation and is critical for proteome maintenance in the nucleus.

Main Text: Cells have evolved complex quality control mechanisms that operate under normal growth conditions and during stress to maintain protein homeostasis (proteostasis) and prevent the formation of potentially toxic aggregates (*1-4*). Subcellular compartments are equipped with specialized stress response pathways (*5-7*) and vary in stress vulnerability (*8-10*). The nuclear proteome is enriched in proteins containing intrinsically disordered or low complexity sequences (*11, 12*). These metastable proteins do not populate a thermodynamically stable folded state and tend to aggregate upon conformational stress (*13-15*). Indeed, various neurodegenerative disorders associated with protein aggregation, such as amyotrophic lateral sclerosis (ALS) and Huntington's disease, are characterized by the presence of intranuclear inclusions (*16-20*).

The nucleus contains several non-membrane bound subcompartments (*21*). The largest of these is the nucleolus which consists of liquid-like phases that do not intermix, giving rise to distinct zones (Fig. 1A and fig. S1A and B) (*22*). Embedded in the outer granular component (GC) phase is the fibrillar center (FC) for the transcription of ribosomal RNA (RNA polymerase I subunit RPA40 as marker). The FC is surrounded by the dense fibrillar component (DFC), which contains the ribonucleoprotein fibrillarin (FBL) (Fig. 1A, and fig. S1A and B). The GC phase is rich in negatively-charged proteins such as nucleophosmin (NPM1) and nucleolin (*23*). NPM1 contains extensive unstructured regions and undergoes liquid-liquid phase separation in vitro (*24, 25*). During stress, Hsp70 and other molecular chaperones accumulate in the nucleolus, presumably to protect unassembled ribosomal proteins against aggregation (*26-28*). Stress-induced transfer of a nuclear model protein to the nucleolus has also been observed (*29*). Here we found that during stress, misfolded proteins entered the liquid-like GC phase of the nucleolus, where irreversible coaggregation of different misfolded protein species was prevented, allowing Hsp70-mediated extraction and refolding (or degradation) upon recovery from stress. In contrast,

disruption of the GC phase caused the formation of stable protein aggregates. Prolonged stress resulted in a transition of the nucleolar matrix from liquid-like to solid and prevented quality control.

Transfer of misfolded protein to the nucleolus upon stress

To investigate the fate of a nuclear protein as it denatures during heat stress (HS), we generated HEK293T cells stably expressing a fusion protein of the thermolabile firefly luciferase and heat-stable GFP carrying an N-terminal nuclear localization signal (NLS-LG) (fig. S1C). NLS-LG was diffusely distributed in the nucleus. Upon incubation at 43 °C (2 hours), a substantial fraction of NLS-LG entered the nucleoli (Fig. 1B). Super-resolution imaging (fig. S1A) (*30, 31*) showed that nucleolar NLS-LG localized to the NPM1-containing GC phase (Fig. 1C, and fig. S1D). Transfer of NLS-LG to the nucleolus was prevented by stabilizing luciferase with the substrate analog 2-phenylbenzothiazole (PBT) (Fig. 1B, and fig. S1E). Thus unfolding was a prerequisite for transfer to the nucleolus. Upon recovery from HS, nucleolar NLS-LG redistributed to the nucleoplasm (Fig. 1B), as shown by inhibiting synthesis of new protein (fig. S1F). More than 60% of NLS-LG was degraded during HS (fig S1G). Notably, the NLS-LG present after recovery showed a higher specific luminescence activity than during HS, indicative of refolding of misfolded protein (fig. S1G).

Hsp70 transferred to nucleoli upon HS (*27-29*), even when NLS-LG was stabilized (fig. S1E). Thus Hsp70 entered the nucleolus either in a complex with endogenous proteins or in free form. Inhibition of the ATPase activity of Hsp70 with the compound VER-155008 (*32*) prevented both Hsp70 and misfolded NLS-LG from exiting the nucleolus during recovery (fig. S2A). Thus nucleolar Hsp70 is involved in refolding and repartitioning NLS-LG (and presumably other metastable proteins) to the nucleoplasm. Indeed, misfolded cytosolic carboxypeptidase Y*-

mCherry (CC*) (*33*) also accumulated in nucleoli when its degradation was inhibited (fig. S2B). Thus the nucleolus serves as a storage compartment for a subset of misfolded proteins under proteotoxic stress conditions, preserving them in a state competent for refolding or degradation.

Misfolded proteins in the nucleolus have low mobility

5   We next analyzed the mobility of NLS-LG in the GC phase of the nucleolus by recording fluorescence recovery after photobleaching (FRAP). To compare the mobility of folded and misfolded proteins within the nucleolus, we fused a nucleolar targeting sequence (*34*) to NLS-LG, generating the protein No-LG (fig. S1C). A large fraction of No-LG constitutively localized to the nucleolus in the absence of stress and in the presence of the luciferase stabilizer PBT (Fig.

10   1D, and fig. S2, C and D), thus behaving as a functional nucleolar protein. No-LG in the nucleolus showed complete FRAP (Fig. 1, D and E, and fig. S3A) and a similar mobility as the liquid-like GFP-NPM1 (Fig. 1F, and fig. S3B) (*22*). HS resulted in a more complete localization of No-LG to the nucleolus, an increased nucleolar concentration of No-LG (1.37 +/- 0.13 fold, n=3), and a shift to a markedly reduced mobility (Fig. 1, D and E, and figs. S2, C and D, and

15   S3A). In contrast, presence of PBT during HS preserved the high mobility of No-LG (Fig. 1, D and E, and fig. S3A). Thus, unfolding changed the interaction of luciferase with the GC phase. The larger hydrodynamic radius of unfolded luciferase may also contribute to the lower mobility. Consistently, the mobility of nucleolar GFP (No-GFP) (figs. S1C, and S2C), remained unchanged upon heat stress (Fig. 1G).

20   HS also induced the formation of an immobile fraction of GFP-NPM1 (~30% of total) (Fig. 1F, and fig. S3B), which returned to normal mobility upon recovery (fig. S3, B and C). Similar observations were made for nucleolin (GFP-NCL) (fig. S3, B and C). This suggested an association with unfolded (or misfolded) proteins that altered GC mobility. In support of this

notion, expression of nucleolar luciferase (as a fusion with mScarlet; No-LS) further increased the immobile fraction of GFP-NPM1 upon HS (Fig. 1F, and fig. S3B), suggesting that the amount of immobile GC protein correlated with the load of misfolded protein. In contrast, folded No-LS in control conditions had no effect on GFP-NPM1 mobility (Fig. 1F, and fig. S3B).

Indeed, endogenous NPM1 associated (directly or indirectly) with NLS-LG or No-LG upon HS by co-immunoprecipitation, but not in the absence of stress (fig. S3D). Thus, unfolding of luciferase enhanced the association with the GC, consistent with a fraction of liquid-like NPM1 and nucleolin adopting a less dynamic state. Inhibiting Hsp70 activity completely inhibited the stress-denatured No-LG from recovery to normal mobility (Fig. 1E, and fig. S3, A and E).

Because No-LG remained localized to the nucleolus after refolding, this finding suggested that refolding mediated by Hsp70 was initiated in the nucleolus and was coupled with the mobilization of luciferase. Thus upon proteotoxic stress, misfolded proteins immersed into the nucleolus, where they associated with GC proteins thereby converting part of the liquid-like GC phase to a state of low mobility (Figure 1F, and fig. S3, B and C). Mobility was reestablished during recovery in an Hsp70-dependent manner, concomitant with refolding.

Endogenous proteins reversibly enter the nucleolus upon stress

To identify the endogenous proteins that enter the GC phase of the nucleolus upon stress, we performed GFP-NPM1 pulldown experiments followed by quantitative proteomics. We identified ~200 proteins that associated with NPM1 specifically upon HS, including numerous proteins of nucleoplasm and nucleolus, as well as some cytosolic proteins (Fig. 2A, fig. S4A and B, and Table S1). Thus the stress-protective GC phase is accessible to proteins from both outside and within the nucleolus.

Nucleolin was also enriched in the NPM1 pulldown, but not the DFC marker fibrillarin (fig. S4C), suggesting an enhanced association between NPM1 and nucleolin under heat stress, consistent with their reduced mobility (Fig. 1F, and fig. S3, B and C). More than 400 proteins of the nucleoplasm or nucleolus were not enriched upon HS (fig. S4, A and C, and Table S1). Thus, the proteins that entered the GC phase constituted a thermally sensitive subproteome. Indeed, these proteins were enriched in disordered and low complexity sequences (fig. S4D), hallmarks of metastable structure. Their accumulation in the GC phase was reversible, while inhibition of Hsp70 preserved the association with NPM1 for most proteins (Fig. 2, A and B, fig. S5A, and Tables S1-S3). Additional proteins associated with NPM1 upon Hsp70 inhibition during recovery (Fig. 2, A and B, and Tables S1 to S3).

We confirmed the reversible accumulation in the nucleolus for the proteins CDK1 and BRD2, which associated with NPM1 upon HS (Fig. 2, C and D, figs. S4C, and S5, B and C, and Table S1). A small but detectable fraction of total cellular Hsp70 also coprecipitated with NPM1 upon HS (fig. S5C), suggesting that associations with both Hsp70 and misfolded protein may contribute to forming the low mobility GC fraction (Fig. 1, E and F, and fig. S3, B and C).

Functional relevance of the nucleolus in quality control

To explore the physiological significance of the nucleolus as a quality control compartment, we disrupted the nucleolar organization. Treating cells with a low concentration of the RNA polymerase I inhibitor actinomycin D (Act D) caused nucleolar disassembly and the release of NPM1 into the nucleoplasm (Fig. 3A) (*35, 36*). NPM1 lost its liquid-like properties as judged by its fast mobility (fig. S6A). NLS-LG was diffusely distributed in the nucleus of Act D treated cells in the absence of stress but formed aggregate foci upon HS (Fig. 3A). These foci did not colocalize with NPM1. They resolved only slowly and inefficiently during recovery (Fig. 3, A

and B) and sequestered Hsp70 for hours after removal of stress (fig. S6B). The terminally

misfolded CC* also formed persistent aggregates in Act D treated cells, when proteasome

function was inhibited (fig. S6, C and D). Thus transport to the phase-separated GC compartment

of the nucleolus was required to maintain misfolded proteins in a state competent for refolding or

degradation once proteotoxic stress was relieved.

The NLS-LG in nucleoplasmic aggregates of Act D treated cells was less mobile than nucleolar

NLS-LG (Fig. 3C). Moreover, the nucleoplasmic foci were positive for amyloid (cross β

structure)-specific dyes, in contrast to NLS-LG in the nucleolus (Fig. 3D, and fig. S6E).

Consistent with an amyloid-like state, the concentration of NLS-LG in nucleoplasmic foci was

~3-fold higher than in the nucleolus (Fig. 3E). When nucleoli were disrupted, HS also caused

endogenous proteins to form amyloid-like foci (fig. S6, F and G). Thus entry of misfolded

proteins into the nucleolus prevented amyloid-like aggregation.

We next analyzed the effect of the nucleolar environment on the model protein β17. This small

β-sheet protein undergoes amyloidogenic aggregation and forms fibrils in vitro (*37*). Targeting

β17 to the nucleus (NLS-β17) results in its accumulation in the nucleolus and a reduced toxicity

compared to cytosolic β17 aggregates (*8*). To determine whether the nucleolar environment was

responsible for this protective effect, we targeted β17 to the nucleoplasm by expressing it with

the C-terminal nuclear localization signal, PY (fig. S7A) (*38*). β17-PY formed foci in the

nucleoplasm, whereas NLS-β17 accumulated in the GC phase of the nucleolus (Fig. 4A). Note

that the NLS apparently functioned as a nucleolar targeting (or retention) signal in the sequence

context with β17, but not in context with LG or GFP (Fig. 1B, and fig. S2C). The function of the

two localization sequences was position-independent (fig. S7A). The nucleoplasmic β17-PY

aggregates were 3-times more concentrated than nucleolar NLS-β17 (Fig. 4B). Importantly, β17-PY was more toxic than NLS-β17 (Fig. 4C), indicating that localization to the nucleolus reduced toxicity (*8*). The PY sequence per se did not confer toxicity (Fig. 4C, and fig. S7B). As expected, nucleolar β17 variants but not nucleoplasmic β17-PY associated with NPM1 (fig. S7C). Moreover, NLS-β17-GFP was significantly more mobile than β17-GFP-PY (fig. S7, D and E), while disrupting the GC phase with Act D rendered NLS-β17-GFP less mobile (fig. S7, D and E).

Amyloid-like aggregates exert their toxic effect in part by co-aggregating and sequestering essential, metastable proteins (*8, 39-41*). Indeed, the nucleoplasmic β17-PY aggregates sequestered NLS-LG upon HS, thereby preventing NLS-LG from entering the nucleolus (Fig. 4D). Nucleolar NLS-β17 had no such effect, and did not prevent repartitioning of NLS-LG to the nucleoplasm upon recovery (Fig. 4D). Thus, the GC phase of the nucleolus had the capacity to simultaneously store different proteins and allowed them to undergo selective renaturation.

Accumulation of misfolded proteins in the nucleolus did not interfere with ribosome biogenesis, as nucleolar NLS-β17 did not interfere with the assembly and export of YFP-tagged 40S ribosomal protein S2 (RPS2-YFP) to the cytosol (fig. S7, F and G) (*42*). In contrast, nucleoplasmic aggregates of β17-PY caused co-aggregation of RPS2-YFP and nuclear retention (fig. S7, F and G).

Limitations of nucleolar quality control

To explore the capacity of the nucleolus for incorporating misfolded proteins, we exposed cells to prolonged stress. We observed a significant increase in nucleolar volume during the first 2 hours of HS (Fig. 5A), presumably reflecting the influx of misfolded proteins. The nucleoli lost

their liquid droplet-like appearance and adopted irregular shapes (fig. S8, A and B), suggestive

of a transition to a hardened state. Indeed, the mobile fraction of GFP-NPM1 decreased markedly

during prolonged HS (Fig. 5B, and fig. S8, C and D). To further assess these changes, we stained

NLS-LG expressing cells with the amyloid-specific dye AmyT and observed a distinct nucleolar

staining developing over time (Fig. 5C). The foci formed during extended HS dissolved only

slowly upon recovery (fig. S8E). Apparently, prolonged stress exhausted the storage capacity of

the nucleolus for misfolded proteins, resulting in a transition to a solid, aggregated state.

Expression of C9orf72 encoded dipeptide repeat proteins (DPRs) is a possible cause of familiar

ALS and frontotemporal dementia (FTD) (*43-45*). These peptides cause nucleolar dysfunction by

modulating the liquid-like properties of the nucleolus (*19, 20*). We expressed the DPR-protein

PR_{175}-GFP along with nuclear luciferase (NLS-LS). PR_{175}-GFP incorporated efficiently into the

GC phase of the nucleolus (Fig. 5D) (*19, 20*), resulting in reduced mobility of a fraction of

mScarlet-NPM1 (fig. S9A). NLS-LS entered the nucleolus during HS and co-localized with

PR_{175}-GFP, but failed to repartition during recovery (Fig. 5D), remaining arrested in the

nucleolus for hours (fig. S9B). In contrast, control cells expressing No-GFP allowed normal

NLS-LS repartitioning (Fig. 5D, and fig. S9B). Thus nucleolar DPR protein leads to a

breakdown of nucleolar quality control, which may contribute to the cellular pathology in ALS

and FTD.

Conclusions

The liquid-like GC phase of the nucleolus functions as a non-membrane bound protein quality

control compartment (Fig. 5E). It is characterized by a remarkable chaperone-like capacity to

prevent irreversible aggregation of misfolded proteins, facilitating refolding during recovery

from stress. Misfolded proteins associate with nucleolar proteins including NPM1, thereby

converting a fraction of the GC phase to a less dynamic state (Fig. 5E). The association of

misfolded proteins with the GC phase is regulated by the chaperone Hsp70, which is required for

refolding (Fig. 5E). While nucleoplasmic proteins exit the nucleolus upon refolding, nucleolar

proteins resume their functional state. However, the capacity of the nucleolus to store misfolded

proteins is limited and prolonged stress causes aberrant phase behavior associated with the

danger of irreversible aggregation (Fig. 5E). Moreover, disease related DPR proteins impair the

ability of the nucleolus to reversibly store misfolded proteins, a mechanism that may contribute

to neurodegenerative pathology.

References and Notes:

1. W. E. Balch, R. I. Morimoto, A. Dillin, J. W. Kelly, Adapting proteostasis for disease intervention. *Science* **319**, 916-919 (2008).

2. T. Gidalevitz, E. A. Kikis, R. I. Morimoto, A cellular perspective on conformational disease: the role of genetic background and proteostasis networks. *Curr Opin Struct Biol* **20**, 23-32 (2010).

3. E. M. Sontag, R. S. Samant, J. Frydman, Mechanisms and Functions of Spatial Protein Quality Control. *Annu Rev Biochem* **86**, 97-122 (2017).

4. R. Higuchi-Sanabria, P. A. Frankino, J. W. Paul, 3rd, S. U. Tronnes, A. Dillin, A Futile Battle? Protein Quality Control and the Stress of Aging. *Dev Cell* **44**, 139-163 (2018).

5. T. Shpilka, C. M. Haynes, The mitochondrial UPR: mechanisms, physiological functions and implications in ageing. *Nat Rev Mol Cell Biol* **19**, 109-120 (2018).

6. P. Walter, D. Ron, The unfolded protein response: from stress pathway to homeostatic regulation. *Science* **334**, 1081-1086 (2011).

7. A. Korennykh, P. Walter, Structural basis of the unfolded protein response. *Annu Rev Cell Dev Biol* **28**, 251-277 (2012).

8. A. C. Woerner *et al.*, Cytoplasmic protein aggregates interfere with nucleocytoplasmic transport of protein and RNA. *Science* **351**, 173-176 (2016).

9. L. Vincenz-Donnelly *et al.*, High capacity of the endoplasmic reticulum to prevent secretion and aggregation of amyloidogenic proteins. *EMBO J* **37**, 337-350 (2018).

10. E. Rousseau *et al.*, Targeting expression of expanded polyglutamine proteins to the endoplasmic reticulum or mitochondria prevents their aggregation. *Proc Natl Acad Sci U S A* **101**, 9648-9653 (2004).

11.   J. S. Andersen *et al.*, Nucleolar proteome dynamics. *Nature* **433**, 77-83 (2005).

12.   Z. M. March, O. D. King, J. Shorter, Prion-like domains as epigenetic regulators, scaffolds for subcellular organization, and drivers of neurodegenerative disease. *Brain Res* **1647**, 9-18 (2016).

13.   A. J. Baldwin *et al.*, Metastability of native proteins and the phenomenon of amyloid formation. *J Am Chem Soc* **133**, 14160-14163 (2011).

14.   S. Raychaudhuri *et al.*, Interplay of acetyltransferase EP300 and the proteasome system in regulating heat shock transcription factor 1. *Cell* **156**, 975-985 (2014).

15.   R. D. Jones, R. G. Gardner, Protein quality control in the nucleus. *Curr Opin Cell Biol* **40**, 81-89 (2016).

16.   A. von Mikecz, Pathology and function of nuclear amyloid. Protein homeostasis matters. *Nucleus* **5**, 311-317 (2014).

17.   C. G. Chung, H. Lee, S. B. Lee, Mechanisms of protein toxicity in neurodegenerative diseases. *Cell Mol Life Sci*, (2018).

18.   K. Mori *et al.*, The C9orf72 GGGGCC repeat is translated into aggregating dipeptide-repeat proteins in FTLD/ALS. *Science* **339**, 1335-1338 (2013).

19.   I. Kwon *et al.*, Poly-dipeptides encoded by the C9orf72 repeats bind nucleoli, impede RNA biogenesis, and kill cells. *Science* **345**, 1139-1145 (2014).

20.   K. H. Lee *et al.*, C9orf72 Dipeptide Repeats Impair the Assembly, Dynamics, and Function of Membrane-Less Organelles. *Cell* **167**, 774-788 e717 (2016).

21.   J. E. Sleeman, L. Trinkle-Mulcahy, Nuclear bodies: new insights into assembly/dynamics and disease relevance. *Curr Opin Cell Biol* **28**, 76-83 (2014).

22.   M. Feric *et al.*, Coexisting Liquid Phases Underlie Nucleolar Subcompartments. *Cell* **165**, 1686-1697 (2016).

23.   M. Biggiogera *et al.*, Nucleolar distribution of proteins B23 and nucleolin in mouse preimplantation embryos as visualized by immunoelectron microscopy. *Development* **110**, 1263-1270 (1990).

24.   D. M. Mitrea *et al.*, Self-interaction of NPM1 modulates multiple mechanisms of liquid-liquid phase separation. *Nat Commun* **9**, 842 (2018).

25.   J. K. Box *et al.*, Nucleophosmin: from structure and function to disease development. *BMC Mol Biol* **17**, 19 (2016).

26.   J. M. Velazquez, S. Lindquist, hsp70: nuclear concentration during environmental stress and cytoplasmic storage during recovery. *Cell* **36**, 655-662 (1984).

27.   W. J. Welch, J. R. Feramisco, Nuclear and nucleolar localization of the 72,000-dalton heat shock protein in heat-shocked mammalian cells. *J Biol Chem* **259**, 4501-4513 (1984).

28.   H. Pelham, M. Lewis, S. Lindquist, Expression of a Drosophila heat shock protein in mammalian cells: transient association with nucleoli after heat shock. *Philos Trans R Soc Lond B Biol Sci* **307**, 301-307 (1984).

29.   E. A. Nollen *et al.*, Dynamic changes in the localization of thermally unfolded nuclear proteins associated with chaperone-dependent protection. *Proc Natl Acad Sci U S A* **98**, 12038-12043 (2001).

30.   J. Schnitzbauer, M. T. Strauss, T. Schlichthaerle, F. Schueder, R. Jungmann, Super-resolution microscopy with DNA-PAINT. *Nat Protoc* **12**, 1198-1228 (2017).

31. S. Strauss *et al.*, Modified aptamers enable quantitative sub-10-nm cellular DNA-PAINT imaging. *Nat Methods* **15**, 685-688 (2018).

32. R. Schlecht *et al.*, Functional analysis of Hsp70 inhibitors. *PLoS One* **8**, e78443 (2013).

33. S. H. Park *et al.*, PolyQ Proteins Interfere with Nuclear Degradation of Cytosolic Proteins by Sequestering the Sis1p Chaperone. *Cell* **154**, 134-145 (2013).

34. A. Birbach, S. T. Bailey, S. Ghosh, J. A. Schmid, Cytosolic, nuclear and nucleolar localization signals determine subcellular distribution and activity of the NF-kappaB inducing kinase NIK. *J Cell Sci* **117**, 3615-3624 (2004).

35. M. Chen, P. Jiang, Altered subcellular distribution of nucleolar protein fibrillarin by actinomycin D in HEp-2 cells. *Acta Pharmacol Sin* **25**, 902-906 (2004).

36. T. Dousset *et al.*, Initiation of nucleolar assembly is independent of RNA polymerase I transcription. *Mol Biol Cell* **11**, 2705-2717 (2000).

37. M. W. West *et al.*, De novo amyloid proteins from designed combinatorial libraries. *Proc Natl Acad Sci U S A* **96**, 11211-11216 (1999).

38. J. Gal *et al.*, Nuclear localization sequence of FUS and induction of stress granules by ALS mutants. *Neurobiol Aging* **32**, 2323 e2327-2340 (2011).

39. H. Olzscha *et al.*, Amyloid-like aggregates sequester numerous metastable proteins with essential cellular functions. *Cell* **144**, 67-78 (2011).

40. M. S. Hipp, S. H. Park, F. U. Hartl, Proteostasis impairment in protein-misfolding and -aggregation diseases. *Trends Cell Biol* **24**, 506-514 (2014).

41. Y. J. Zhang *et al.*, C9ORF72 poly(GA) aggregates sequester and impair HR23 and nucleocytoplasmic transport proteins. *Nat Neurosci* **19**, 668-677 (2016).

42.   T. Wild *et al.*, A protein inventory of human ribosome biogenesis reveals an essential function of exportin 5 in 60S subunit export. *PLoS Biol* **8**, e1000522 (2010).

43.   M. DeJesus-Hernandez *et al.*, Expanded GGGGCC hexanucleotide repeat in noncoding region of C9ORF72 causes chromosome 9p-linked FTD and ALS. *Neuron* **72**, 245-256 (2011).

44.   I. Gijselinck *et al.*, A C9orf72 promoter repeat expansion in a Flanders-Belgian cohort with disorders of the frontotemporal lobar degeneration-amyotrophic lateral sclerosis spectrum: a gene identification study. *Lancet Neurol* **11**, 54-65 (2012).

45.   A. E. Renton *et al.*, A hexanucleotide repeat expansion in C9ORF72 is the cause of chromosome 9p21-linked ALS-FTD. *Neuron* **72**, 257-268 (2011).

46.   R. Gupta *et al.*, Firefly luciferase mutants as sensors of proteome stress. *Nat Methods* **8**, 879-884 (2011).

47.   D. S. Bindels *et al.*, mScarlet: a bright monomeric red fluorescent protein for cellular imaging. *Nat Methods* **14**, 53-56 (2017).

48.   T. la Cour *et al.*, Analysis and prediction of leucine-rich nuclear export signals. *Protein Eng Des Sel* **17**, 527-536 (2004).

49.   S. May *et al.*, C9orf72 FTLD/ALS-associated Gly-Ala dipeptide repeat proteins cause neuronal toxicity and Unc119 sequestration. *Acta Neuropathol* **128**, 485-503 (2014).

50.   J. Schindelin *et al.*, Fiji: an open-source platform for biological-image analysis. *Nat Methods* **9**, 676-682 (2012).

51.   C. A. Schneider, W. S. Rasband, K. W. Eliceiri, NIH Image to ImageJ: 25 years of image analysis. *Nat Methods* **9**, 671-675 (2012).

52. J. Ollion, J. Cochennec, F. Loll, C. Escude, T. Boudier, TANGO: a generic tool for high-throughput 3D image analysis for studying nuclear organization. *Bioinformatics* **29**, 1840-1841 (2013).

53. D. Legland, I. Arganda-Carreras, P. Andrey, MorphoLibJ: integrated library and plugins for mathematical morphology with ImageJ. *Bioinformatics* **32**, 3532-3534 (2016).

54. S. E. Ong, M. Mann, A practical recipe for stable isotope labeling by amino acids in cell culture (SILAC). *Nat Protoc* **1**, 2650-2660 (2006).

55. J. R. Wisniewski, D. F. Zielinska, M. Mann, Comparison of ultrafiltration units for proteomic and N-glycoproteomic analysis by the filter-aided sample preparation method. *Anal Biochem* **410**, 307-309 (2011).

56. S. Tyanova *et al.*, The Perseus computational platform for comprehensive analysis of (prote)omics data. *Nat Methods* **13**, 731-740 (2016).

57. W. Huang da, B. T. Sherman, R. A. Lempicki, Systematic and integrative analysis of large gene lists using DAVID bioinformatics resources. *Nat Protoc* **4**, 44-57 (2009).

58. W. Huang da, B. T. Sherman, R. A. Lempicki, Bioinformatics enrichment tools: paths toward the comprehensive functional analysis of large gene lists. *Nucleic Acids Res* **37**, 1-13 (2009).

59. J. J. Ward, L. J. McGuffin, K. Bryson, B. F. Buxton, D. T. Jones, The DISOPRED server for the prediction of protein disorder. *Bioinformatics* **20**, 2138-2139 (2004).

60. J. C. Wootton, S. Federhen, Analysis of compositionally biased regions in sequence databases. *Methods Enzymol* **266**, 554-571 (1996).

61. S. S. Agasti *et al.*, DNA-barcoded labeling probes for highly multiplexed Exchange-PAINT imaging. *Chem Sci* **8**, 3080-3091 (2017).

Author contributions: F.F. designed and performed most of the experiments. R.G. carried out initial experiments. F.S. and T.Sc. carried out the high resolution imaging. R.K. supervised the proteomic analysis and S.Ti. and J.C. analyzed sequence properties of NPM1 associated proteins. R.J. designed and supervised the high resolution imaging experiments. F.U.H. and M.S.H. initiated and supervised the project and wrote the paper with input from F.F. and the other authors.

Competing interests:

J.C. is also affiliated with the Department of Biological and Medical Psychology, Faculty of Psychology at the University of Bergen, Bergen, Norway

Data and materials availability: Data from the mass spectrometry analysis described in this manuscript can be found in the supplementary materials.

Fig. 1. Misfolded proteins transiently accumulate in the GC phase of the nucleolus during stress. (**A**) Schematic representation and 3D rendered DNA-PAINT (*30, 31*) super-resolution image of a HeLa cell nucleolus under normal growth condition. NPM1 (GC, red), FBL (DFC, white) and RPA40 (FC, cyan). See also fig. S1, A and B (**B**) HEK293T cells stably expressing NLS-LG were treated with DMSO (mock) or PBT before 2 h of heat stress (+HS), followed by recovery for 2 h (+HS +Rec). Control cells were maintained at 37 °C (-HS). Cells were stained for endogenous NPM1 (red), nuclei are marked by a dashed circle. (**C**) Super-resolution imaging of HEK293T cells expressing NLS-LG after HS treatment, with staining for GFP, endogenous NPM1, FBL and RPA40. See fig. S1D for –HS control. (**D**) No-LG in the nucleolus without (– HS) and with (+HS) heat stress in presence or absence of PBT. Before bleaching (Pre), immediately after bleaching (Bleach) and 2 s after bleaching. (**E** to **G**) FRAP analysis of No-LG (E), GFP-NPM1 (F) and No-GFP (G). No-LG experiments (E) with PBT treatment (empty circles) or DMSO (full circles) as a control. GFP-NPM1 experiments (F) with co-transfection of No-LS where indicated. For the -HS condition (green), cells were maintained at 37 °C during acquisition. For +HS experiments (red), cells were incubated at 43 °C for 1 h before acquisition and maintained at 43 °C during acquisition. For the No-LG recovery experiment (E, right graph, blue), cells were subjected to HS and 1 h recovery (+HS +Rec; full circles), followed by FRAP. Hsp70 was inhibited with VER-155008 before shifting cells to recovery (+HS +Rec +VER; empty circles) (*32*). CHX was present during recovery. The graphs display corrected and normalized FRAP curves with double exponential fits. Curves are given as mean values ± SD; n ≥ 4 biological repeats representing at least 12 different cells. The first 150 s after photo-bleaching are shown. Quantification of No-LG and GFP-NPM1 mobility is shown in fig. S3, A and B respectively. Scale bars (A, C, D) 1 μm, (B) 10 μm.

Fig. 2. GFP-NPM1 reversibly associates with endogenous proteins. (**A**) Number of GFP-NPM1 associated proteins (see Table S1). GFP-NPM1 was transiently expressed in SILAC-labeled HEK293T cells before exposure to heat stress (+HS), followed by recovery (+HS +Rec) or recovery in the presence of Hsp70 inhibitor (+HS +Rec +VER). Control cells remained at 37 °C (-HS). Anti-GFP immunoprecipitates from cell lysates were analyzed by mass spectrometry. Proteins that were ≥ 2-fold enriched upon +HS over the -HS sample in at least 3 of 4 independent experiments were defined as being associated with GFP-NPM1 (see Table S1). Numbers of GFP-NPM1 associated proteins are shown. (**B**) Hsp70 inhibition prevents reversibility of GFP-NPM1 associations. Venn diagrams show distribution of GFP-NPM1 associated proteins under the conditions analyzed in (A). (**C**) Bromodomain-containing protein 2 (BRD2) reversibly accumulates in the nucleolus. HEK293T cells were treated as described above. Cells were immunostained for endogenous NPM1 and BRD2. Nuclei are marked with a dashed line. Representative images of 3 biological repeats are shown. Scale bar, 10 μm. (**D**) Partitioning of BRD2, NLS-LG and Hsp70 between nucleoplasm and nucleoli in HEK293T cells treated as described above. Proteins were detected by immunostaining. Relative concentrations in nucleoplasm and nucleolus were quantified by measuring relative fluorescence intensities in 57 to 145 cells per condition across 3 biological repeats. *P*-values from two-sided *t*-tests are shown (**$P \leq 0.05$, ***$P \leq 0.001$).

Fig. 3. The nucleolar environment prevents irreversible protein aggregation. (**A**) HEK293T cells expressing NLS-LG (green) were treated with actinomycin D (Act D) where indicated, followed by incubation with and without HS and recovery as in Fig. 1B. Cells were immunostained for NPM1 (red), nuclei are marked by a dashed circle. (**B**) HEK293T cells expressing NLS-LG were treated as in (A) and recovery was monitored over 2 h. Cells with nuclear NLS-LG foci were counted during recovery and expressed as percentage of total. Data are displayed as mean ± SD; 453 to 693 cells were counted per time point and per condition across 3 biological repeats. *P*-values from two-sided *t*-tests are shown (*$P \leq 0.05$, ***$P \leq 0.001$). (**C**) HEK293T cells expressing NLS-LG were subjected to FRAP analysis. Cells were treated with Act D (empty circles) before HS where indicated. For -HS experiments (green) the nucleoplasmic region was bleached, where NLS-LG localizes at 37 °C. For +HS experiments (red) the nucleolus was bleached (see schematic). On the left, normalized FRAP curves with double exponential fits are shown. Curves are given as mean ± SD; n ≥ 3 biological repeats. On the right, the mobile fraction from the double exponential fit is shown. (**D**) Cells expressing NLS-LG were subjected to Act D treatment where indicated, followed by heat stress (+HS) and stress with recovery (+HS +Rec), and stained with AmyT. Nuclei are marked with a dashed line. (**E**) Concentration of NLS-LG in the nucleolus and in nucleoplasmic aggregates (+Act D) upon heat stress. Statistical significance is based on Mann-Whitney test (***$P \leq 0.001$). 100 measurements per condition across three biological repeats were done. Scale bars 10μm.

Fig. 4. Accumulation in the nucleolus reduces toxicity of amyloidogenic protein and prevents co-aggregation with misfolded luciferase. (**A**) HEK293T cells were transfected with NLS-β17 or β17-PY prior to super-resolution imaging. C-myc (β17, red), NPM1 (cyan) and RPA40 (white). Zoomed images of NLS-β17 in the nucleolus are shown on the right.

(**B**) Density of β17 in the nucleolus (NLS-β17) and in nucleoplasmic aggregates (β17-PY) measured by super-resolution imaging. Data were normalized to the average density of nucleolar NLS-β17. Statistical significance is based on Mann-Whitney test (***$P \le 0.001$). At least 36 and 52 measurements were performed on one representative experiment out of 3 biological repeats for NLS-β17 and β17-PY, respectively. (**C**) HEK293T cells were transfected with the indicated constructs and MTT cell viability assays were performed 4 days after transfection. Data were normalized to cells transfected with empty vector. The mean + SD is given, n $\ge$ 3, *P*-value from two-sided *t*-test is shown (**$P \le 0.01$). (**D**) β17-PY or NLS-β17 were transfected into the NLS-LG expressing HEK293T cell line. 24 h after transfection cells were subjected to HS (+HS) and allowed to recover for 1 h (+HS +Rec) before fixation. Endogenous NPM1 (cyan), c-myc (β17, red). Arrows show NLS-LG sequestration into β17-PY aggregates. Scale bars (A) 1 μm, (D) 10 μm.

Fig. 5. The nucleolus changes phase properties during prolonged stress or accumulation of dipeptide repeat protein. (**A**) HeLa cells were incubated at 43 °C for the times indicated before staining for endogenous NPM1. The average nucleolar volume per nucleus is displayed as a bee-swarm boxplot. Welch's t-test was used to assess significant differences between conditions; the resulting *P*-values are given. Results are from 3 biological repeats representing 155 to 264 analyzed cells per condition. (**B**) NPM1 mobile fraction from FRAP experiments performed with HeLa cells transfected with GFP-NPM1. Cells were subjected to HS for the times indicated prior to and during FRAP measurement, and GFP-NPM1 mobile fractions were calculated. See also fig. S8, C and D. Data are represented as mean + SD of at least 3 biological repeats. *P*-value of two-sided t-test is shown (*$P \leq 0.05$, **$P \leq 0.01$, ***$P \leq 0.001$). (**C**) NLS-LG expressing HEK293T cells were subjected to heat treatment for the indicated times, and stained with AmyT. Nuclei are marked with a dashed line. (**D**) HEK293T cells were co-transfected with NLS-LS and either PR$_{175}$-GFP or the nucleolar control-protein No-GFP. Cells were maintained at 37 °C (-HS) or subjected to heat stress (+HS) and recovery (+HS +Rec). (**E**) Model of nucleolar protein quality control for proteins entering the nucleolus from the nucleoplasm. Misfolded proteins immerse into the liquid-like GC phase of the nucleolus, presumably as a complex with Hsp70 (green), where they associate with GC proteins such as NPM1 (dark blue). There they are stored in an immobile state within the liquid-like GC-phase, accompanied with an expansion of the nucleolus. Mobility is reestablished upon recovery from stress in an Hsp70-dependent manner, allowing refolding or proteasomal degradation in the nucleoplasm. Preventing access to the GC phase, results in amyloid-like aggregation in the nucleoplasm. Upon prolonged stress, the GC phase increasingly transitions towards a more solid state. Misfolded proteins are no longer dispersed but form aggregates with amyloid-like properties. Scale bars 10 μm.
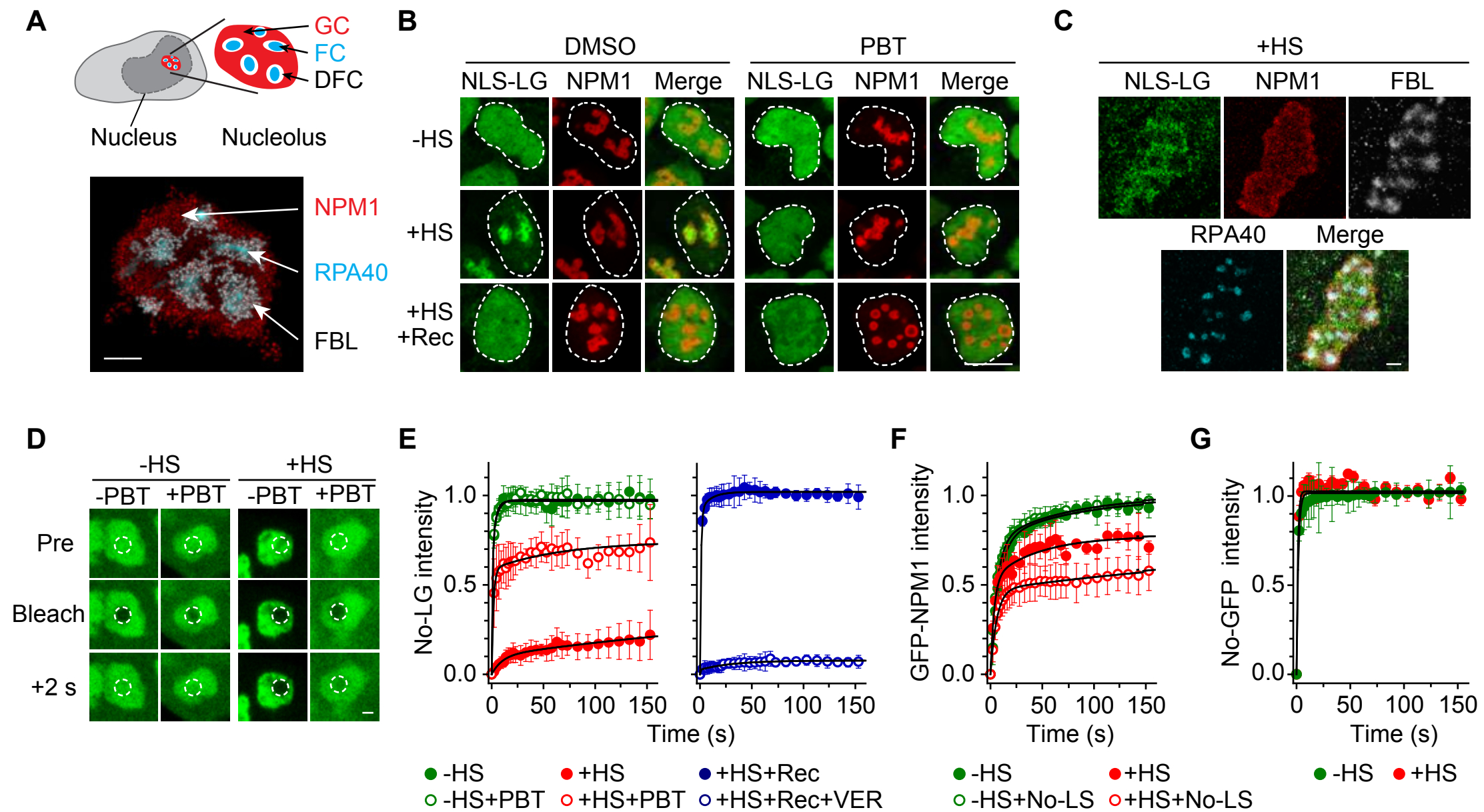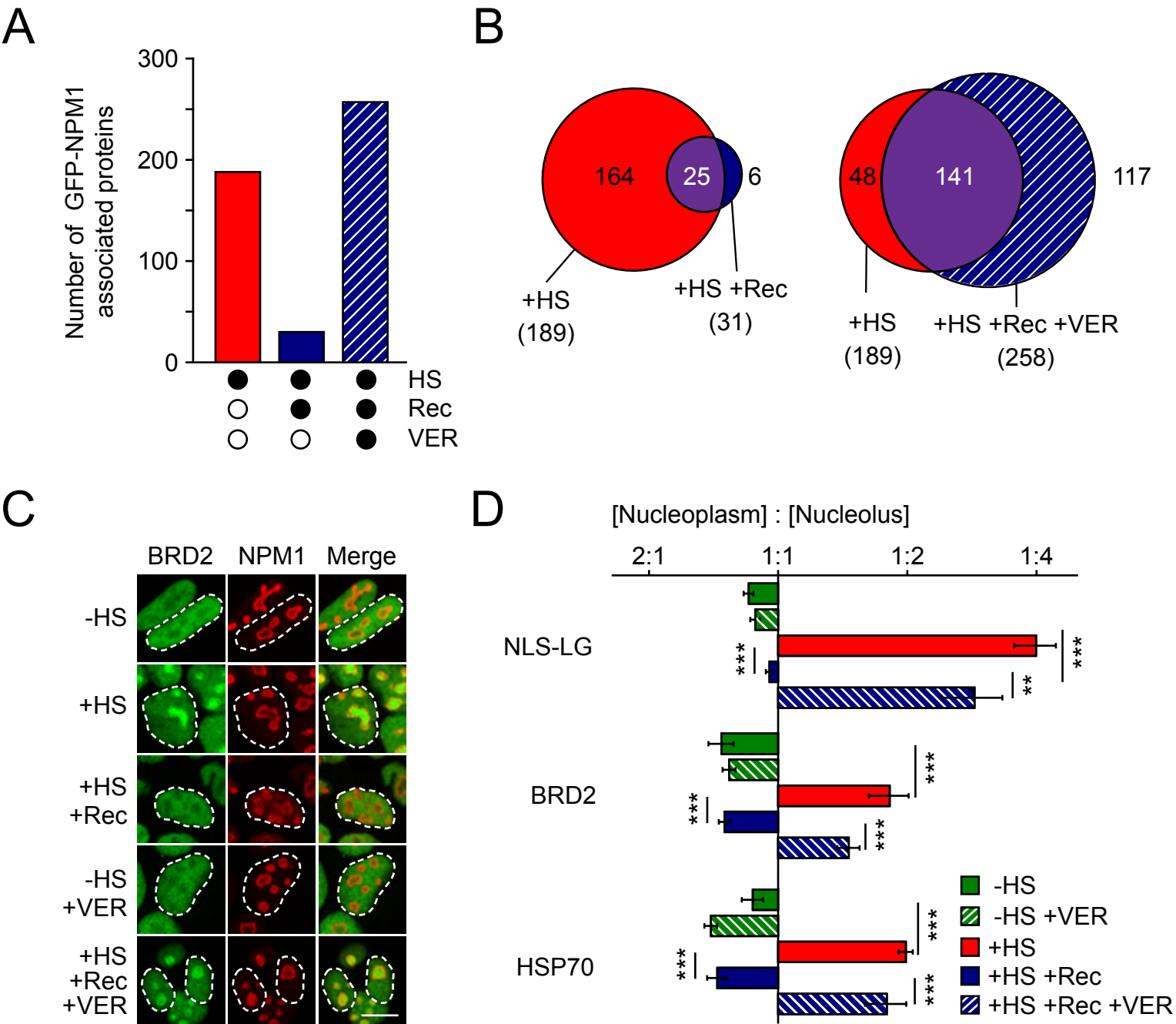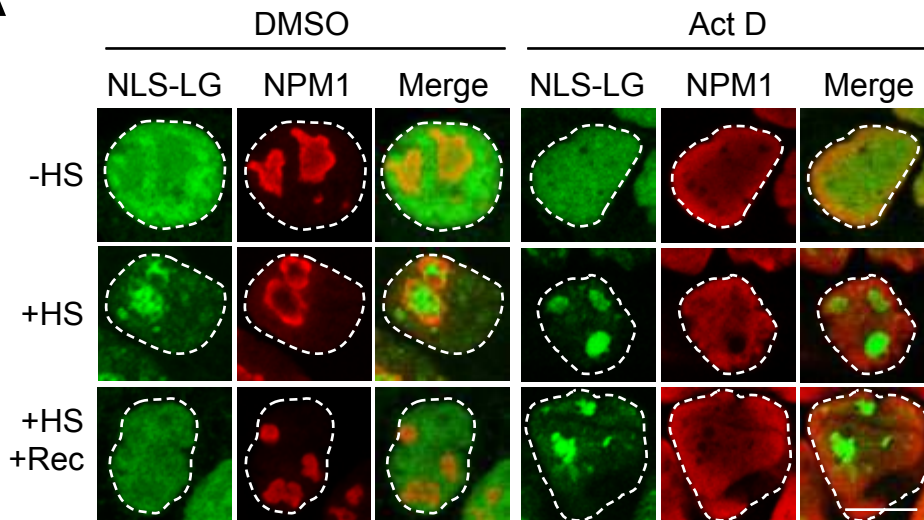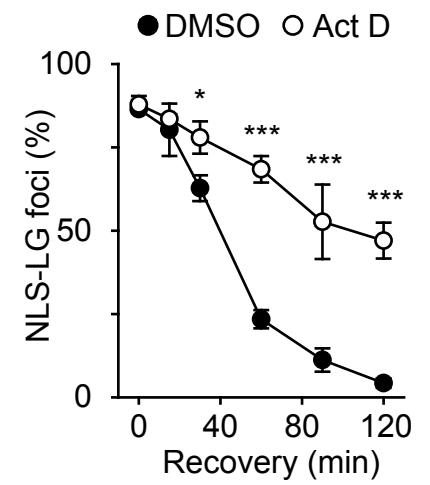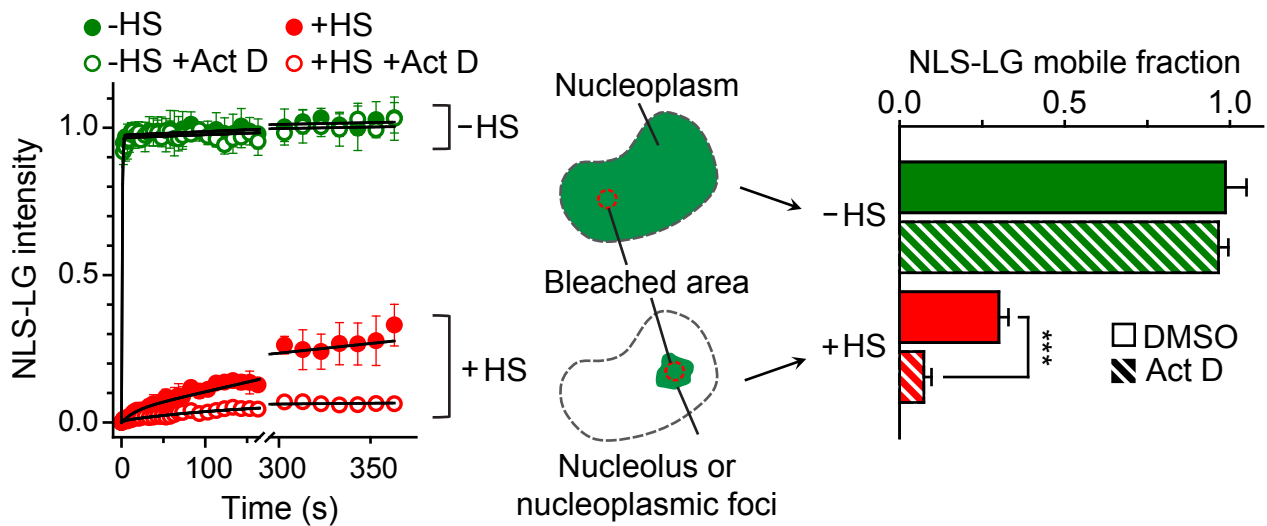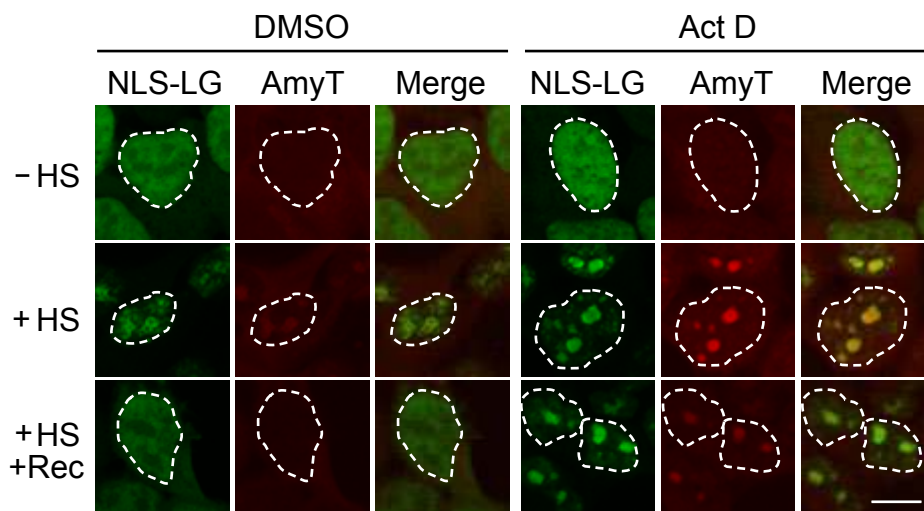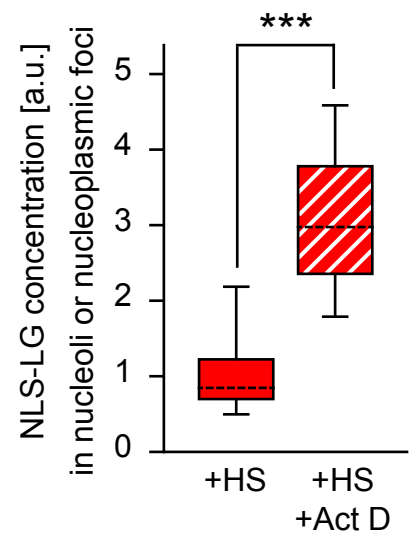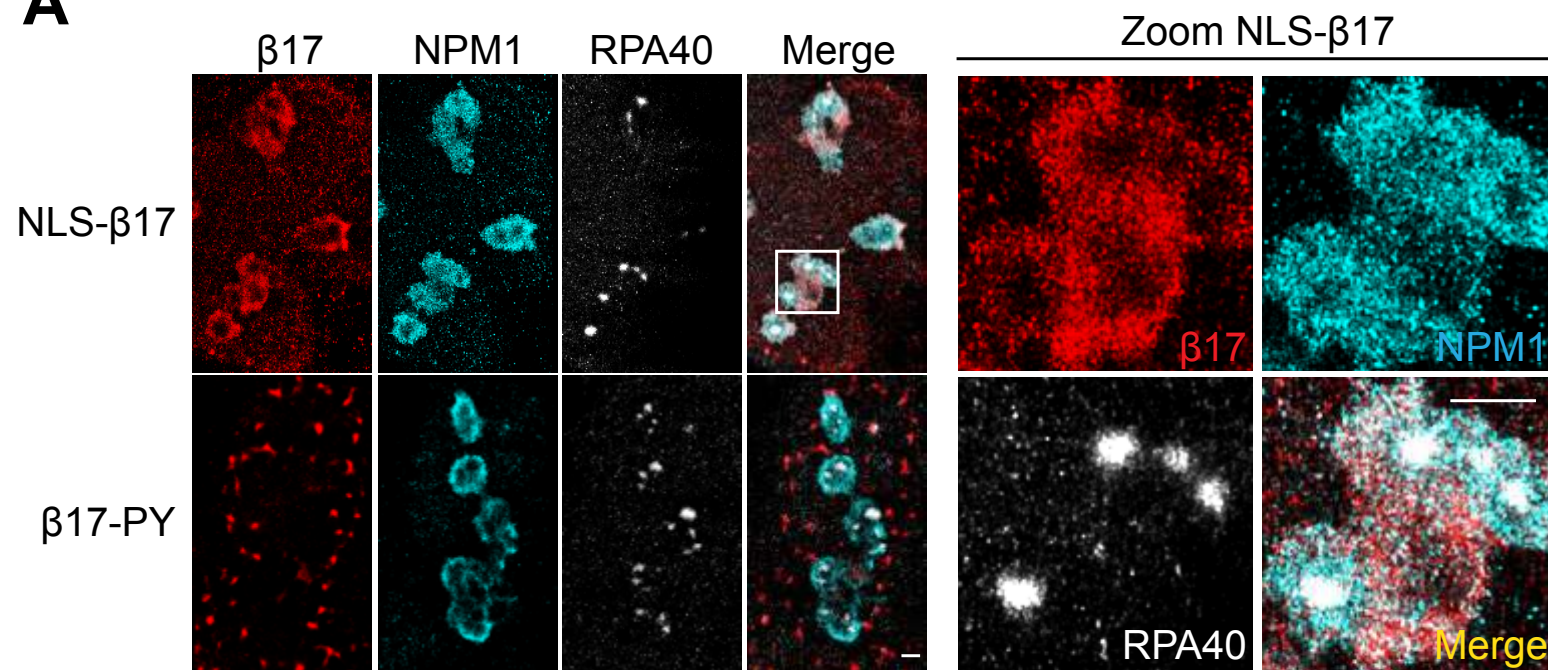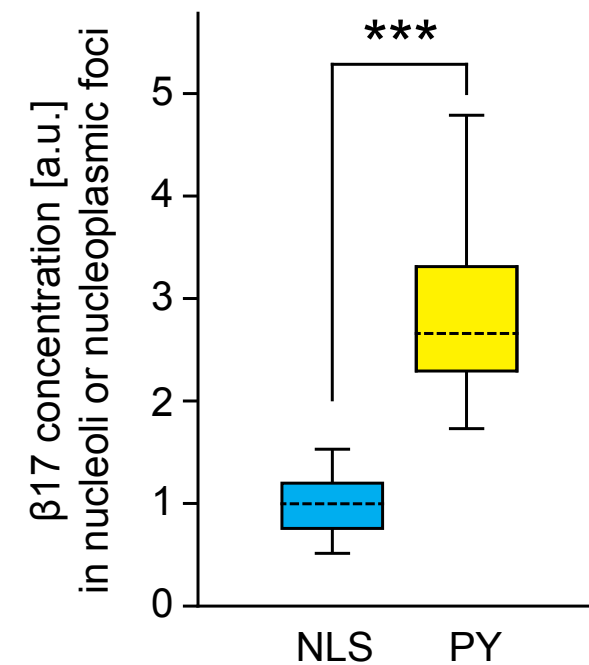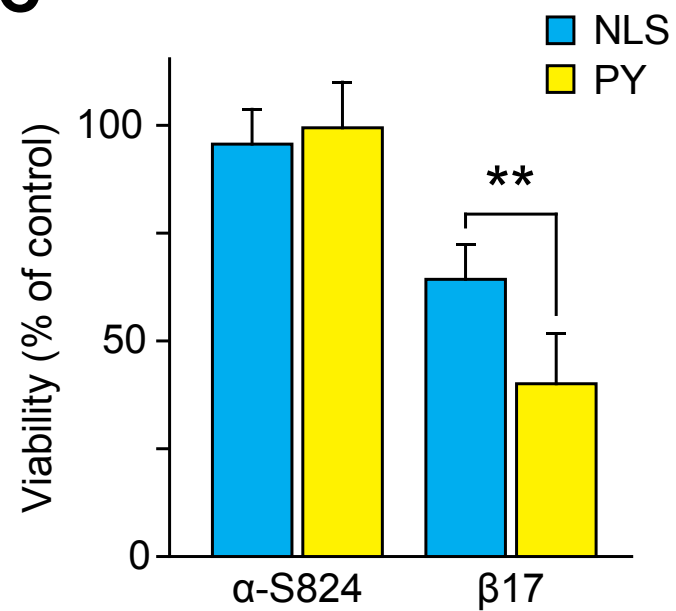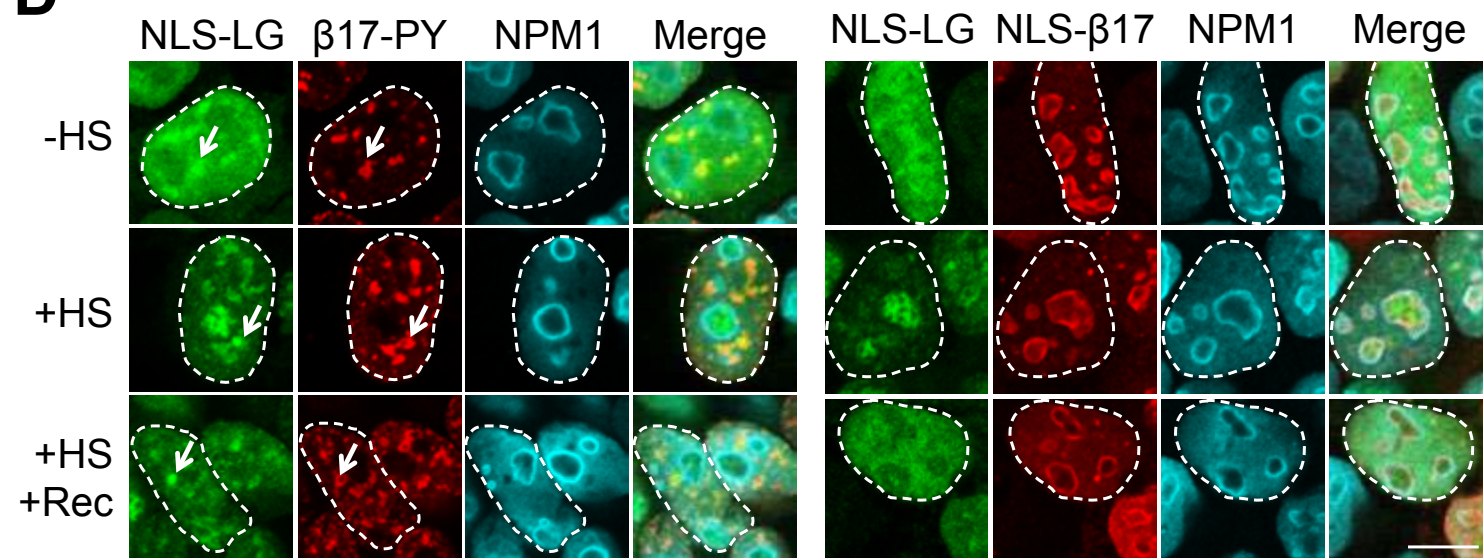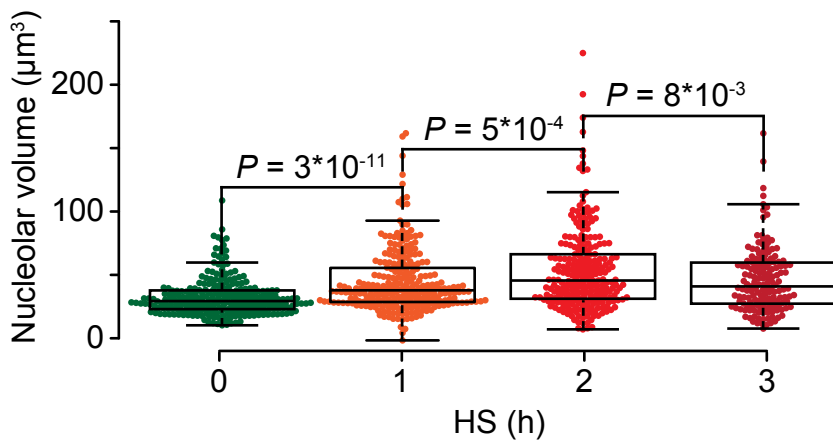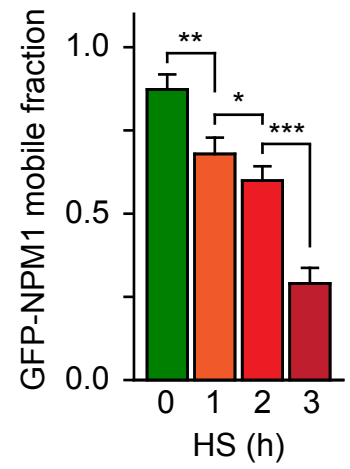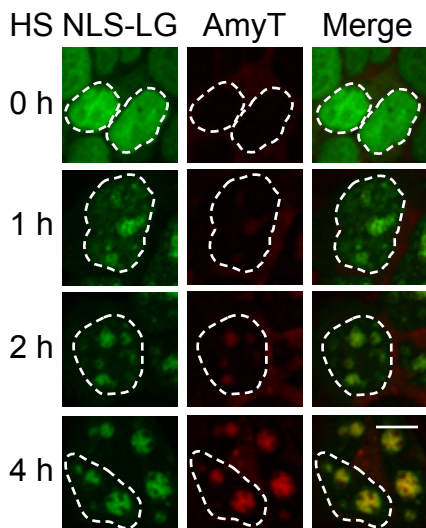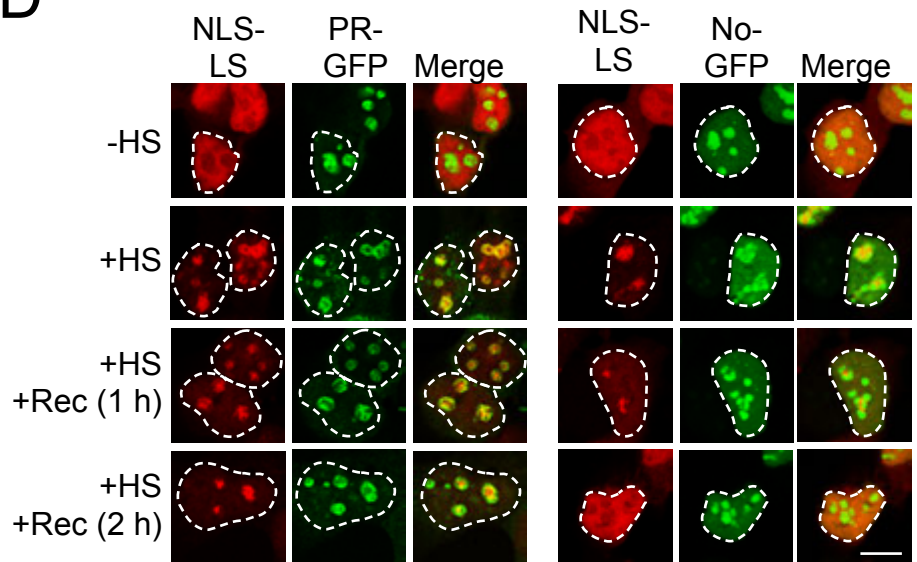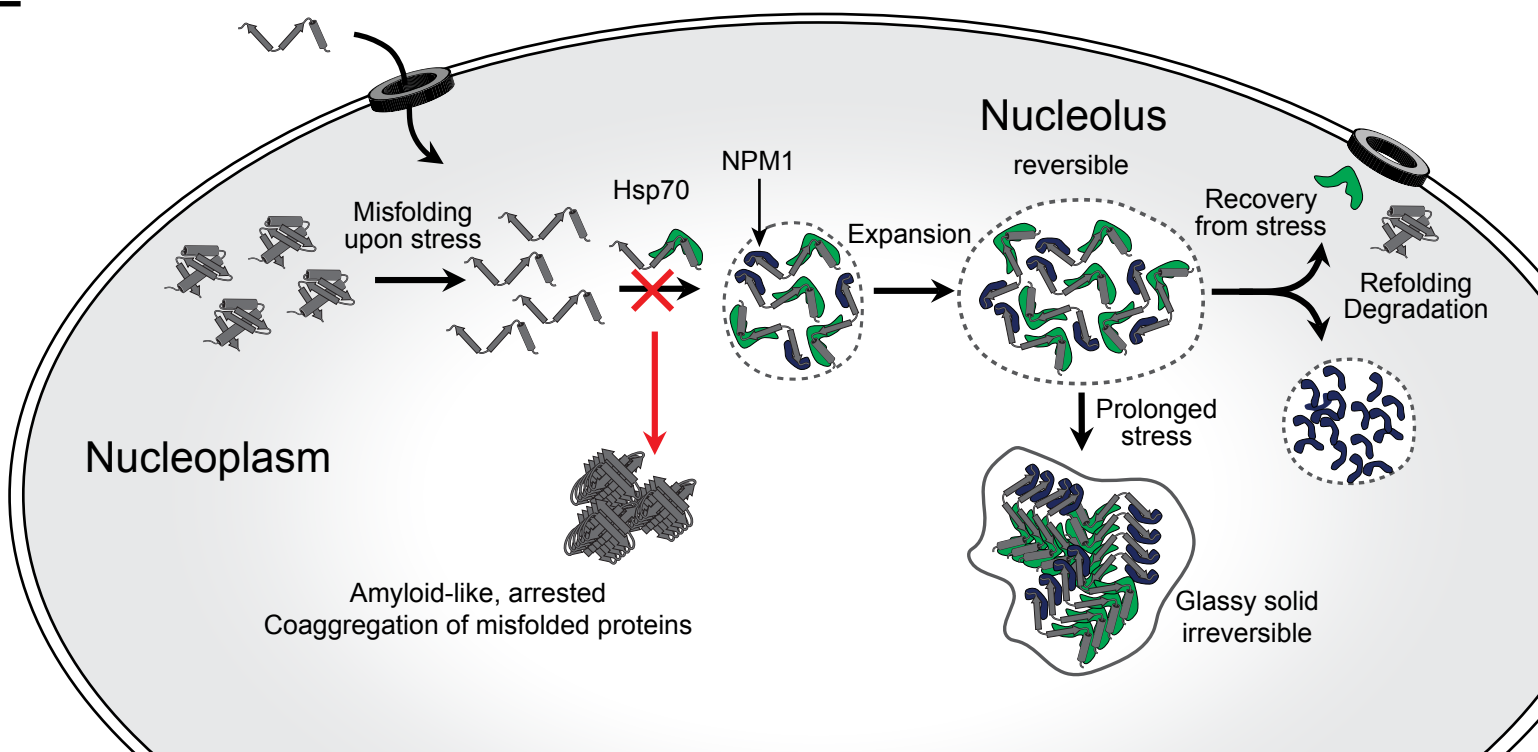
Supplementary Materials for

The nucleolus functions as a phase-separated protein quality control compartment

F. Frottin, F. Schueder, S. Tiwary, R. Gupta, R. Körner, T. Schlichthaerle, J. Cox,
R. Jungmann, F.U. Hartl, M.S. Hipp

correspondence to: uhartl@biochem.mpg.de (F.U.H.); hipp@biochem.mpg.de (M.S.H.);
jungmann@biochem.mpg.de (R.J.)

This PDF file includes:

> Materials and Methods
> Figs. S1 to S9
> Captions for databases S1 to S3

Other Supplementary Materials for this manuscript includes the following:

> Databases S1 to S3 as zipped archives: Frottin et al Table S1-S3.xlsx.zip

Materials and Methods

Cell Culture and transfection

HEK293T and HeLa cells were obtained from ATCC and were maintained at 37 °C
and 5% CO_2 in Dulbecco's modified Eagle's medium (Biochrom KG) supplemented with
10% fetal bovine serum (GIBCO), 100 IU/ml penicillin (GIBCO), 100 UI/ml
streptomycin sulfate (GIBCO), 2 mM L-glutamine (GIBCO) and non-essential amino
acid cocktail (GIBCO). The HEK293T NLS-LG polyclonal cell line was generated with
G418 sulfate (GIBCO) selection and the cell population was further homogenized by
fluorescence assisted cell sorting. The stable line was maintained in the medium
described above supplemented with G418 (100 µg/ml). For heat stress and recovery, cells
were either maintained at 37 °C (-HS), or placed in a 43 °C (+HS) incubator for the
indicated duration, or subjected to heat stress and then transferred back to 37 °C for
recovery (+HS +Rec).

The HeLa RPS2-YFP line was a kind gift from U. Kutay and cells were cultured as
previously described (*42*). RPS2-YFP expression was induced with 125 ng/ml
tetracycline in the growth medium after transfection for 24 h before experiments.
Transient transfections were performed by lipofection with Lipofectamine 2000
(Invitrogen) according to the manufacturer's guidelines. When double transfection was
required, equal amounts of both plasmids were simultaneously transfected.

Chemicals and cell treatments

Chemicals were purchased from Sigma-Aldrich except when stated otherwise. 2-
phenylbenzothiazole (PBT) was used at 40 µg/ml. Actinomycin D (Act D) was used at

100 ng/ml. MG-132 (Cayman Chemical) was used at 10 µM. VER-155008 was used at 50 µM. These previous compounds were dissolved in DMSO as stock solutions before final dilution into growth medium. DMSO concentration never exceeded 1‰ (v/v). For translation inhibition, cycloheximide (CHX) was dissolved in phosphate buffer saline (PBS) and applied at the final concentration of 1 mM. For all non-treated samples, vehicle alone was used as control.

Plasmids

To generate NLS-LG, FlucWT-eGFP (*46*) was PCR amplified and inserted at the 3' end of the duplicated SV40 NLS (DPKKKRKVDPKKKRKV) sequence in the pcDNA3.1/myc-His A plasmid backbone. The c-myc and His tags were excluded with a stop codon. To produce NLS-LS, mScarlet was PCR amplified and introduced between XbaI and BamHI to replace eGFP (*47*). To generate No-LG, the nucleolar localization sequence from the kinase NIK (RKKRKKK) was inserted by site-directed mutagenesis in the linker between the NLS and luciferase sequences and at the C-terminal of eGFP of NLS-LG (*34*). eGFP was exchanged for mScarlet in No-LG to produce No-LS. No-GFP was generated by site-directed deletion of luciferase in the No-LG construct. CC* was produced from CmCh* (*33*) by adding the nuclear export signal at the 5' end of CmCh* by site directed mutagenesis (*33, 48*). The pEGFP-C2 GFP-NPM1 plasmid was a king gift from Xin Wang (Addgene plasmid # 17578). To generate mScarlet-NPM1, eGFP was replaced by mScarlet. The pEF6 PR$_{175}$-GFP expression plasmid was a kind gift from D. Edbauer (*49*).

NLS-β17 and NLS-α-S824 were previously described (*8*). β17-PY and α-S824-PY originate from β17 and α-S824 (*39*) in pcDNA3.1 expression vector. The PY sequence (RGGRGGGDRGGFGPGKMDSRGEHRQDRRERPY) from the protein FUS was inserted in-frame at the C-terminal of β17 and α-S824 by two rounds of site-directed insertion (*38*). PY-β17 was generated by inserting the PY sequence at the N-terminus of β17. β17-NLS was generated by site-directed insertion of the double NLS sequence at the C-terminus of β17. No-β17-PY was generated by inserting the nucleolar localization sequence at the N-terminus of β17-PY. β17-GFP-PY was generated from β17-GFP by site-directed insertion of the PY sequence at the C-terminus of GFP. NLS-β17-GFP was previously described (*8*). All relevant plasmid regions were verified by sequencing.

Antibodies and dyes

The following primary antibodies were used in this study: c-Myc (9E10), Santa Cruz (sc-40); c-Myc-Cy3 (9E10), Abcam (ab24609); GAPDH, Millipore (MAB374); α-Tubulin, Sigma Aldrich (T6199); NPM1, Invitrogen (32-5200); GFP, Roche (11814460001); Fibrillarin, Cell Signaling Technology (#2639); RPA40, Santa Cruz (sc-374443); Hsp70/Hsc70, Stressgen (ADI-SPA820); BRD2, Abcam (ab139690); CDK1, Abcam (ab133327).

The following secondary antibodies were used: Mouse IgG-Alexa488, Cell signaling Technology (#4408); Mouse IgG-Alexa555, Cell signaling Technology (#4408); Rabbit IgG-Alexa555, Cell signaling Technology (#4408); Mouse IgG-Alexa488, Invitrogen (21200); anti-mouse IgG-Peroxidase, Sigma Aldrich (A4416); anti -rabbit IgG-Peroxidase, Sigma Aldrich (A9169).

The amyloid dye AmyTracker 680 (AmyT; Ebba Biotech AB) was used essentially as described in the manufacturer's guidelines. Briefly, cells were fixed in 4% paraformaldehyde in PBS (GIBCO) for 20 min, washed twice with PBS, permeabilized with Triton X-100 0.1 % (v/v) for 5 min, followed by two washes. AmyT was used at 1:500 dilution and incubated with the samples for 1 h at room temperature. Cell were washed and nuclei counterstained with 4', 6-Diamidine-2'-phenylindole dihydrochloride (DAPI). NIAD4 (Biovision) staining was carried out similarly. After permeabilization, cells were incubated with 10 µM NIAD4 for 1 h at room temperature before counterstaining with DAPI. For Amylo-glo (Biosensis) staining, cells were fixed and permeabilized according to the manufacture's guidelines. Then cells were incubated with Amylo-glo (1:200 in 0.9% NaCl) for 15 min. Nuclei were then counterstained with DRAQ5 (Invitrogen) according to the manufacturer's instructions.

Immunofluorescence

Cells were grown on poly-L-lysine coated coverslips (Neuvitro). Cells were fixed with 4% paraformaldehyde in PBS (GIBCO) for 20 min at room temperature before permeabilization for 5 min with Triton X-100 0.1% (v/v) in PBS at room temperature. Samples were blocked with 1% bovine serum albumin in PBS at room temperature for 60 min. Primary antibodies were applied in blocking buffer supplemented with 0.1% Triton X-100 and incubated overnight at 4°C. Appropriate fluorescent secondary antibodies at a dilution of 1:500 were applied after PBS washes for 120 min at room temperature in PBS. Nuclei were counterstained with DAPI before mounting samples with fluorescent compatible mounting medium (DAKO).

<u>Image acquisition and analysis of fixed samples</u>

Confocal microscopy was performed at MPIB Imaging Facility (Martinsried, Germany) on a ZEISS (Jena, Germany) LSM780 confocal laser scanning microscope equipped with a ZEISS Plan-APO 63x/NA1.46 oil immersion objective. In multi-fluorescence samples, a single-stained control sample was used to adjust emission and detection configuration to minimize spectral bleed-through. When fluorescence intensities were directly compared, acquisition settings were kept unchanged and resulting images treated identically. Images were analyzed with ImageJ (Rasband, W.S., National Institutes of Health, USA) and assembled in Adobe Photoshop CC (Adobe Systems Incorporated, Release 19.1.5). A dashed line is used to depict the boundary of the nucleus based on DAPI or DRAQ5 staining.

To count fluorescent protein foci, several confocal images were taken in three independent repeats and were analyzed for visible foci in ImageJ. At least 125 cells were counted across the replicates per condition and time point.

To measure the relative local concentration of NLS-LG, images were acquired using the same microscope settings. Mean GFP fluorescence intensity inside aggregate foci or in nucleoli were measured using ImageJ in 100 cells per conditions across 3 biological repeats.

For imaging cells treated with amyloid-staining dyes, the ZEISS (Jena, Germany) LSM780 confocal laser scanning microscope equipped with a ZEISS Plan-APO 63x/NA1.46 oil immersion objective was used with identical settings for the different experimental conditions. For the experiments in which cells were exposed to prolonged

stress, the background of the AmyT channel was uniformly subtracted in ImageJ using rolling ball background subtraction (radius: 50 pixels) settings.

Volumetric analysis of nucleoli

Image stacks of HeLa cells, subjected to various durations of heat stress and stained for endogenous NPM1, were acquired. Quantification of nucleolar volume was performed using the software ImageJ (*50, 51*), complemented with the default plugins provided by FIJI and with the additional plugins 3D Image Suite (*52*) and MorphoLibJ (*53*). A script was written to repeat the same analysis on all stack images. Each stack was processed twice, first to detect the nuclei and then to detect and measure the nucleoli inside each nucleus. For each processing step, the algorithms used are reported as described in ImageJ, and their parameters are reported in pixels, corresponding to 165 nm in each planar dimension, and to 500 nm in the third dimension. In order to detect the nuclei, the images were pre-processed by first removing the background signal (rolling ball background subtraction, kernel radius: 100), then locally enhancing the contrast (contrast limited adaptive histogram equalization, CLAHE, kernel size: 127), and finally reducing the noise level (3D median filtering, kernel radius: 3). The nuclei were segmented using a local adaptive threshold (Phansalkar method, kernel radius: 150), and their boundaries were rounded by morphological opening (spherical structuring element, radius: 6 along x and y, 1 along z). Nuclei that were only partially imaged in the field of view were excluded from the analysis. Once the location and the approximate extension of nuclei were determined, the original images were processed again to detect the nucleoli inside. First the images were processed to reduce the noise signal, by combining

a Gaussian filter (kernel radius: 1) with a Median filter (kernel radius: 3 along x and y, 1 along z). Then, for each nucleus its central slice was determined as the one with the highest standard deviation of its intensity, and its average intensity was used as a reference to determine the range of slices where to limit the search of nucleoli (average intensity of the slices higher than half the reference intensity). On each selected slice the nucleoli were segmented by Otsu thresholding, after subtracting the background intensity. Adjacent nucleoli were separated by distance transform watershed (distance metric: Borgefors). The results from the analysis of each slice were combined by connected component labeling, to obtain a single segmentation for each nucleolus. The segmented volume of each nucleolus was finally regularized by morphological closing (3D binary label closing, kernel radius: 5 along x and y, 2 along z). Data from the nucleoli quantification are displayed as bee swarm box plots. Center lines show the medians; box limits indicate the 25th and 75th percentiles; whiskers extend 1.5 times the interquartile range from the 25th and 75th percentiles, data points are plotted as circles. Welch's t-test was used to assess statistical significance.

RPS2-YFP partitioning between nucleus and cytoplasm

RPS2-YFP HeLa cells were transfected with the indicated constructs and RPS2-YFP expression was induced for 24 h before cell fixation. β17 and α-S824 protein variants were detected by immunostaining using anti-c-myc antibody and cells counterstained with DAPI. The relative concentration of RPS2-YFP in the nucleus and cytoplasm was quantified by measuring the mean fluorescence intensity in each compartment in at least 150 cells per condition across 3 biological repeats. The fluorescence intensity ratio of

cytoplasm/nucleus was then computed. Fluorescence intensities were acquired using ImageJ. Alternatively, cells with an abnormal RPS-YFP cellular distribution pattern were counted and expressed as percentage of transfected cells.

Partition coefficient between nucleoplasm and nucleoli

HEK293T cells expressing the indicated constructs or non-transfected cells were treated as indicated. Non-transfected cells were immunostained against BRD2 or HSP70. Both transfected and non-transfected cells were immunostained against the indicated nucleolar marker (NPM1 or NCL). Cells were counterstained with DAPI. The relative concentration of the constructs and endogenous proteins in the nucleolus and nucleoplasm was quantified by measuring the mean fluorescence intensity in each compartment in 57-145 cells per condition across 3 biological repeats. The fluorescence intensity ratio of [nucleoplasm] : [nucleolus] was then calculated and plotted using a logarithmic scale. Fluorescence intensities were acquired using ImageJ.

Fluorescence recovery after photobleaching (FRAP) analysis

Cells were grown on poly-L-lysine coated chambered slides (Ibidi) and maintained at the desired temperature (37 °C or 43 °C) and with 5% CO_2 during acquisition. FRAP experiments were performed at MPIB Imaging Facility on a Leica (Leica Microsystems, Wetzlar, Germany) TCS SP8 A0BS confocal laser scanning microscope equipped with a Leica HSX PL APO 63X/NA1.2 water immersion objective. Circular regions of constant size were bleached and monitored overtime for fluorescence recovery. Fluorescence intensity data were corrected for background fluorescence, photobleaching and

normalized using FRAPAnalyser software

(http://actinsim.uni.lu/eng/Downloads/FRAPAnalyser). Resulting FRAP curves were

fitted with double exponential equations for the graphs and exponential fit was used to

extract the mobile fraction and $t_{1/2}$ of fluorescence recovery. A single exponential fit was

used to extract these parameters over the first 100 s of fluorescence recovery or a double

exponential fit was used over the total recovery time when relevant (i.e. plateau not

reached). Individual fittings of each biological replicate were used to obtain the averaged

parameters displayed in bar graphs.

Cell viability assay

HEK293T cells were transfected with the indicated constructs and cell viability was

assessed 96 h after transfection. Viable cells were quantified with the realtime MT cell

viability assay (Promega) according to manufacturer's instructions. Data were normalized

to cells transfected with empty vector. Each repeat is an average of technical triplicates.

Protein analysis by immunoblotting

After SDS-PAGE and protein transfer, immunoblots were developed using

Luminata Forte Western HRP substrate (Millipore) and pictures were acquired with a

LAS-3000 camera system (Fujifilm). AIDA (Raytest) software was used for analysis and

quantitation.

Luciferase specific luminescence activity

For firefly luciferase activity measurements, identical amounts of cells were seeded in 96-well plates. After 48 h, 30 μl of Steady-Glo Luciferase Assay system buffer (Promega) was added to the wells to lyse the cells and incubated for 15 min in the dark at room temperature. Luminescence was then recorded in a luminometer (Berthold Lumat LB9507) (acquisition time, 2 s). In parallel, identical amounts of cells were seeded in 24 well plates to determine the NLS-LG amount. Cells were lysed and boiled in SDS buffer, followed by SDS-PAGE and immunoblotting. Specific luciferase activity was determined by normalizing luminescence intensity by luciferase band intensities quantified from immunoblots by densitometry using the Advanced Image Data Analyzer software (AIDA, Raytest).

Immunoprecipitation

Cells expressing the GFP or c-myc tagged proteins were washed with PBS and lysed in RIPA (radio immunoprecipitation assay buffer containing 1% NP-40, 1% sodium deoxycholate and 0.1% SDS; Thermo Fisher Scientific) buffer supplemented with Protease Inhibitor Cocktail (Roche) and Benzonase Nuclease (Novagen). Samples were sonicated and further incubated for 30 min at 4 °C. Cell debris were removed by centrifugation (10 min; 2,000 g; 4 °C). Protein concentration was measured with Bradford assay (Bio-Rad) and 1 mg of lysate per sample (950 μl) was incubated with 50 μl of anti-GFP or anti-c-myc micro-beads (Miltenyi biotech) for 1 h with agitation. Samples were applied to pre-equilibrated μMAC columns (Miltenyi biotech) and washed 3 times with the RIPA buffer and 1 time with PBS before elution with gel loading buffer.

Eluates were then analyzed by SDS-PAGE and immunoblotting (NLS-LG; No-LG; GFP-NPM1; β17) or mass spectrometry analysis (GFP-NPM1).

Proteomic analysis

Sample preparation. Quantitative GFP-NPM1 and GFP interactome analysis was performed using the SILAC method (*54*). Custom DMEM (PAA) was used for SILAC labeling of HEK293T cells: arginine- and lysine-free DMEM was supplemented with 10% dialyzed FCS (PAA), 100 IU ml^{-1} penicillin G, 100 μg ml^{-1} streptomycin sulphate, 2 mM L-glutamine and non-essential amino acid cocktail (Gibco). To prepare light (L), medium (M), and heavy (H) media, the following amino acids were added: for L, Arg0 and Lys0 (arginine and lysine, Sigma); for M, Arg6 and Lys4 (Arg-^{13}C6 and Lys-4,4,5,5-D4, Silantes); for H, Arg10 and Lys8 (Arg-^{13}C6,^{15}N4 and Lys-^{13}C6,^{15}N2, Silantes). Efficient incorporation of the isotopes was verified by mass spectrometry. Cells were harvested for analysis 24 h after transfection with GFP-NPM1. The experiment included two different labelling schemes to prevent labelling artifacts. For the heat stress experiment the first two repeats were labeled as follows: GFP-NPM1 +HS, H and GFP-NPM1 -HS, M. The last two repeats were labeled as follows: GFP-NPM1 +HS, M and GFP-NPM1 -HS, L (Table S1). For the recovery experiment, the first two repeats were labeled as follows: GFP-NPM1 +HS +Rec, M and GFP-NPM1 -HS, L. The last two repeats were labeled as follows: GFP-NPM1 +HS +Rec, H and GFP-NPM1 -HS, L (Table S2). For the recovery experiment in presence of the Hsp70 inhibitor VER-155008, the first two repeats were labeled as follows: GFP-NPM1 +HS +Rec +VER, H and GFP-NPM1 -HS, L. The last two repeats were labeled as follows: GFP-NPM1 +HS +Rec

+VER, M and GFP-NPM1 -HS, L (Table S3). Immunoprecipitation of GFP was performed as described above. Eluates of immunoprecipitates of labeled cells were mixed in equal ratio. Protein reduction, alkylation and tryptic digestion was performed using the filter-aided sample preparation (FASP) method (*55*).

LC-MS/MS. After desalting with a C18 column, tryptic peptides were dissolved in 5% formic acid and analyzed by nanoLC-MS/MS using an EASY-nLC 1000 (Thermo Fisher Scientific) nano liquid chromatography system coupled to a Q-Exactive mass spectrometer (Thermo Fisher Scientific) or an EASY-nLC 1200 nanoHPLC (Thermo Fisher Scientific) coupled to a Q-Exactive HF (Thermo Fisher Scientific). Samples were injected onto a home-made 25 cm silica reversed-phase capillary column (New Objective) packed with 1.9 µm ReproSil-Pur C18-AQ (Dr. Maisch GmbH). Samples were loaded on the column by the nLC autosampler at a flow rate of 0.5 µl per minute. No trap column was used. Peptides were separated by a 190-min gradient of 5–30% between buffer A (0.1% formic acid in water) and buffer B (0.1% formic acid in 80% acetonitrile) at a flow rate of 300 nl/min. MS/MS analysis was performed with standard settings using cycles of one high resolution (60000 FWHM setting) MS scan followed by MS/MS scans of the 15 most intense ions with charge states of 2 or higher at a resolution setting of 15000 FWHM.

Data analysis and statistics. Protein identification and SILAC based quantitation was performed with MaxQuant (version 1.3.0.5) using default settings. The UNIPROT Homo sapiens database (version 2017-04-06) was used for protein identification. MaxQuant uses a decoy version of the specified UNIPROT database to adjust the false discovery rates for proteins and peptides below 1%. Four independent biological repeats

were performed, including two different labeling schemes. MaxQuant ratios were used for the analysis of interactor enrichment. One sample t-test P-Value of the enrichment factor ($S0 = 0$) and gene ontology cell compartment terms were retrieved using Perseus (*56*) (see Table S1). Interactors of GFP-NPM1 were defined as proteins enriched by at least 2-fold in at least 3 of 4 biological repeats. Gene ontology term enrichment analysis was performed using DAVID (version 6.8; thresholds: Count 2, EASE 0.1) (*57, 58*). Frequency and the longest disordered sequences and low complexity regions (LCRs) were identified using the predictor DISOPRED (*59*) and the SEG-algorithm (*60*), respectively. The non-parametric Mann-Whitney U test, calculated using Python, was used to assess statistical significance.

Super-resolution Microscopy

Imaging Buffer. For imaging, buffer C containing PBS pH 8, 500 mM NaCl, 1× Trolox, 1× PCA, 1× PCD was used (*30*). Alignment and drift correction was performed using 90 nm gold particles (Cytodiagnostics) incubated for 5 min prior image acquisition.

Antibody preparation for coupling. Sodium azide from primary antibody stock solution was removed in four dialysis steps into a PBS reservoir in 10 kDa Slide-A-Lyzer MINI dialysis units (Thermo) at 4 ºC under constant stirring. For removal of protein stabilizers, antibodies were selectively purified via protein G agarose (Thermo). 100 µl of protein G resin slurry was added to a 2 ml tube. The slurry was centrifuged for 15 s at 10,000 g and the supernatant was removed. For a total of three subsequent washes, 50 µl of PBS at pH 7.2 was added to the resin and resuspended by gently flicking the tube. After centrifugation and supernatant removal, the antibody was added to the protein G

14

slurry in a 2 ml tube and incubated for 90 min on a tube rotator at room temperature. Then, the solution was centrifuged in a spin cup column for 1 min at 1,000 *g*. The flow through was collected in a separate tube and the slurry was washed 10 times with 100 µl of PBS at pH 7.2 with subsequent collections of the flow-through in separate tubes. Then, 100 µl of IgG elution buffer (0.1 M glycine-HCl at pH 2.7) was added and incubated under mixing for 5 min. Afterwards the spin cup was centrifuged for 1 min at 1,000 *g* to elute the bound IgG antibody. The flow through was neutralized by adding 3-5 µl of 1 M Tris at pH 9.0 and the spin cup was transferred to a fresh tube. Elution buffer was added to the slurry and incubated for 5 min with subsequent centrifugation, collection and neutralization of the flow-through. This procedure was repeated 3 more time. Elution fractions were pooled after determination of IgG protein concentration. Final buffer exchange and sample concentration was performed via 100 kDa Amicon spin filter units (Merck) and antibody samples were subjected to DNA conjugation. Subsequent labeling of purified antibodies with thiolated DNA (MWG Eurofins) was performed as described before (*61*).

SOMAmer preparation. SOMAmer reagents for GFP imaging were prepared as described before (*31*).

Immunostaining. HEK293T cells containing NLS-β17 and β17-PY and HeLa cells for prolonged heat stress experiments were fixed with 2.4% PFA (Electron Microscopy Science) for 30 min. All other cells were fixed with 1.4% PFA for 30 min. Next, samples were blocked and permeabilized using 3% BSA (Sigma Aldrich) and 0.25% Triton-X100 (Carl Roth) for 2 h. Immunostaining was performed in PBS buffer containing 3% BSA and 0.1% Triton-X100.

For HEK293T cells containing NLS-β17 and β17-PY (Figure 3A), samples were incubated with primary mouse anti-RPA40 antibody (Santa Cruz, cat. Sc-374443, dilution 1:250) and primary goat anti-myc antibody (abcam, cat. ab9132, dilution 1:500) over night at 4 ºC. Next, samples were stained with P6 DNA sequence-coupled anti-mouse secondary antibody (Jackson Immuno Research, dilution 1:200), and a P1 DNA sequence-coupled anti-goat antibody (Jackson, dilution 1:100) for 2 h at room temperature. Then, samples were incubated with a P5 DNA sequence-coupled primary anti-NPM1 antibody (Thermo, cat. 32-5200, dilution 1:500) at 4 ºC overnight.

For HEK293T cells expressing NLS-LG, samples were incubated with primary mouse anti-RPA40 (Santa Cruz, cat. Sc-374443, dilution 1:250) antibody and rabbit anti-FBL (abcam, cat. ab5821, dilution 1:200) antibody over night at 4 ºC. Next, samples were stained with X66 DNA sequence-coupled anti-mouse secondary antibody (Jackson, dilution 1:200) and X61 DNA sequence-coupled anti-rabbit secondary antibody (Jackson, dilution 1:200) for 2 h at room temperature. Then, samples were incubated with P5 DNA sequence-coupled primary anti-NPM1 antibody for 6 h at 4 ºC. Finally, cells were incubated with the GFP-SOMAmer (SomaLogic, see SOMAmer preparation) with a P1 docking site at 4 ºC overnight.

For HeLa cell imaging samples were incubated with primary mouse anti-RPA40 (Santa Cruz, cat. Sc-374443, dilution 1:250) antibody and rabbit anti-FBL (abcam, cat. ab5821, dilution 1:200) antibody over night at 4 ºC. Next, samples were stained with X66 DNA sequence-coupled anti-mouse secondary antibody (Jackson, dilution 1:200) and X61 DNA sequence-coupled anti-rabbit (Jackson, dilution 1:200) for 2 h at room temperature.

Finally, samples were incubated with P5 DNA sequence-coupled primary mouse anti-NPM1 antibody (Thermo, cat. 32-5200) for 6 h at 4 ºC.

DNA-PAINT docking and imager sequences

Name	DNA Sequence (AB = Antibody, Soma = SOMAmer)	Imager sequence
P1	5'-AB-TT-ATACATCTA-3'	5'-CTAGATGTAT-Cy3b-3'
P1	Cy3-5'-ATACATCTA-TT-Soma-3'-inverted-dT	5'-Cy3b-CTAGATGTAT-3'
P3	5'-AB-TT-TCTTCATTA-3'	5'-GTAATGAAGA-Cy3b-3'
P5	5'-AB-TT-TCAATGTAT-3'	5'-CATACATTGA-Cy3b-3'
P6	5'-AB-TT-TTAGGTAAA-3'	5'-CTTTACCTAA-Cy3b-3'
X61	5'-AB-TT-TCCTCAATTA -3'	5'-TAATTGAGGA-Cy3b-3'
X66	5'-AB-TT-TAAATTTCC-3'	5'-GGGAAATTTA-Cy3b-3'

Super-resolution microscopy setup. Fluorescence imaging was carried out on an inverted Nikon Eclipse Ti microscope (Nikon Instruments) with the Perfect Focus System, applying an objective-type total internal reflection fluorescence (TIRF) configuration with an oil-immersion objective (Apo SR TIRF 100×, NA 1.49, Oil). For excitation a 561 nm laser (200 mW, Coherent Sapphire) was used. The laser beam was passed through cleanup filters (ZET561/10, Chroma Technology) and coupled into the microscope objective using a beam splitter (ZT561rdc, Chroma Technology). Fluorescence light was spectrally filtered with an emission filter (ET600/50m and

ET575lp, Chroma Technology) and imaged on a sCMOS camera (Andor Zyla 4.2) without further magnification, resulting in an effective pixel size of 130 nm (after 2×2 binning).

Imaging of HeLa cell nucleoli. For every round of imaging 20,000 frames at a frame rate of 5 Hz were acquired. The camera was set to a readout rate of 200 MHz and a Pixel depth of 16 Bit. The laser power was set to 40 mW, which translates to an intensity at the sample plane of 0.9 kW/cm^2. Imager strands were all labeled with Cy3b dyes. In the first round, the imager with the sequence P5 was used at a concentration of 0.5 nM to visualize NPM1. In the second round, the imager with the sequence X66 was used at a concentration of 1.5 nM to visualize RPA40. In the third round, the imager with the sequence P3 was used at a concentration of 2 nM to visualize FBL. All imaging was performed in Buffer C with Trolox, PCA and PCD. Between the imaging rounds, free floating imager were washed away using PBS until no residual blinking was observed.

Imaging of NLS-LG - Control. For every round of imaging 15,000 frames at a frame rate of 6.66 Hz were acquired. The camera was set to a readout rate of 540 MHz and a Pixel depth of 16 Bit. Imager strands were all labeled with Cy3b dyes. In the first round, the imager with the sequence P1 was used at a concentration of 2 nM to visualize luciferase via the GFP at a laser power of 29 mW which translates to an intensity at the sample plane of 0.65 kW/cm^2. The remaining rounds were imaged at a laser power of 35 mW which translates to an intensity at the sample plane of 0.8 kW/cm^2. In the second round, the imager with the sequence P5 was used at a concentration of 0.5 nM to visualize NPM1. In the third round, the imager with the sequence X61 was used at a concentration of 2 nM to visualize FBL. In the last round, the imager with the sequence

X66 was used at a concentration of 1.5 nM to visualize RPA40. All imaging was performed in buffer C with 1× Trolox, 1× PCA and 1× PCD. Between the imaging rounds, free floating imager was washed away using ~10 ml of 1× PBS until no residual blinking was observed.

Imaging of NLS-LG - Heat stress. For every round of imaging 15,000 frames at a frame rate of 6.66 Hz were acquired. The camera was set to a readout rate of 200 MHz and a Pixel depth of 16 Bit. Imager strands were all labeled with Cy3b dyes. In the first round, the imager with the sequence P1 was used at a concentration of 2 nM to visualize luciferase via the GFP at a laser power of 20 mW, which translates to an intensity at the sample plane of 0.45 kW/cm^2. The remaining rounds were imaged at a laser power of 44 mW, which translates to an intensity at the sample plane of 1 kW/cm^2. In the second round, the imager with the sequence P5 was used at a concentration of 0.5 nM to visualize NPM1. In the third round, the imager with the sequence X61 was used at a concentration of 2 nM to visualize FBL. In the last round, the imager with the sequence X66 was used at a concentration of 1.5 nM to visualize RPA40. All imaging was performed in buffer C with 1× Trolox, 1× PCA and 1× PCD. Between the imaging rounds, free floating imager was washed away using ~10 ml of 1× PBS until no residual blinking was observed.

Imaging of NLS-β17 and β17-PY. For every round of imaging 10,000 frames at a frame rate of 6.66 Hz were acquired. The camera was set to a readout rate of 540 MHz and a Pixel depth of 16 Bit. The laser power was set to 40 mW which translates to an intensity at the sample plane of 0.9 kW/cm^2. Imager strands were all labeled with Cy3b dyes. In the first round, the imager with the sequence P1 was used at a concentration of

0.5 nM to visualize β17 via the c-myc tag. In the second round, the imager with the sequence P6 was used at a concentration of 1.5 nM to visualize RPA40. In the third round, the imager with the sequence P5 was used at a concentration of 0.5 nM to visualize NPM1. All imaging was performed in buffer C with 1× Trolox, 1× PCA and 1× PCD. Between the imaging rounds, free floating imager was washed away using ~10 ml of 1× PBS until no residual blinking was observed.

Imaging of nucleoli upon prolonged heat stress. For every round of imaging 15,500 frames at a frame rate of 6.66 Hz were acquired. The camera was set to a readout rate of 540 MHz and a Pixel depth of 16 Bit. The laser power was set to 35 mW which translates to an intensity at the sample plane of 0.8 kW/cm^2. Imager strands were all labeled with Cy3b dyes. The imager with the sequence P5 was used at a concentration of 0.5 nM to visualize NPM1. All imaging was carried out in buffer C with 1× Trolox, 1× PCA and 1× PCD. Between the imaging rounds, free floating imager was washed away using ~10 ml of 1× PBS until no residual blinking was observed.

Image post processing and β17 density analysis. The image post processing was performed using Picasso (*30*). For the spatial relative density analysis of the β17, circular regions with a diameter of 520 nm for NLS-β17 and 260 nm for β17-PY were selected using the Picasso pick tool and normalized by area for relative density. The number of binding events (which is a proxy for concentration) for all picked regions was computed. Then, an average from all picks from the same region (e.g. NLS-β17 or β17-PY) was calculated. This average number of events was then normalized to the number for NLS-β17.

3D rendering of HeLa cell nucleoli. DNA-PAINT super-resolution data were processed (localized, fitted, drift corrected, aligned and exported) with the Picasso software. From here, data were imported into Imaris (Version 9.2.1) for 3D rendering using the "Super-resolution data to Image" function. The voxel size was set to 15 nm x 15 nm x 15 nm. Next, a 15 nm Gaussian blur was applied. For the rendering a maximum intensity projection (MIP) rendering was used.

Statistics

Except otherwise stated significant differences were assessed using unpaired Student's t-test using the following criteria $*P \leq 0.05$, $**P \leq 0.01$ and $***P \leq 0.001$.
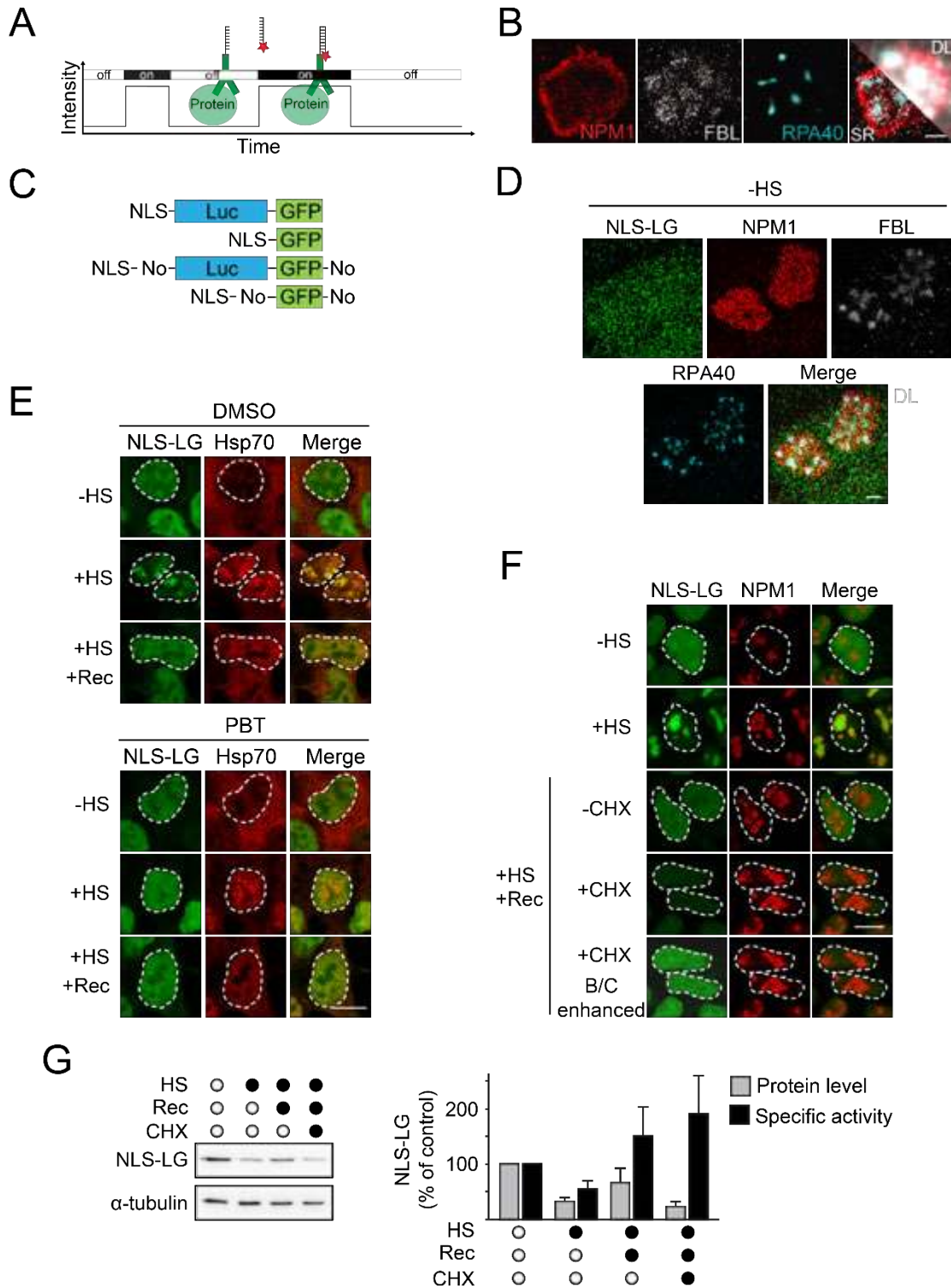
Fig. S1

Properties of nucleolar NLS-LG. (**A**) Schematic of DNA-PAINT. Fluorescent dye-labeled DNA molecules ('imager strands') bind transiently to their complementary targets ('docking strands') attached to antibodies binding a protein of interest (*36*). The transient binding of imager strands is detected as 'blinking', illustrated by the schematic intensity versus time trace. This blinking allows the reconstruction of super-resolved images. (**B**) Single probe images of the super-resolution image of the 3D-rendered nucleolus shown in Fig. 1A. GC marker, NPM1 (red); DFC marker, FBL (white); FC marker, RPA40 (cyan). Super-resolution (SR) and diffraction limited (DL) images are shown as a merge. (**C**) Schematic representation of the firefly luciferase (Luc) and control protein constructs used in this study. (**D**) Super-resolution imaging of HEK293T cells expressing NLS-LG under control conditions (-HS) (see Fig. 1C for +HS). (**E**) Stabilizing NLS-LG upon HS does not influence Hsp70 transfer into the nucleolus. NLS-LG expressing HEK293T cells were treated as in Fig. 1B. Cells were analyzed for NLS-LG and stained for Hsp70. (**F**) NLS-LG expressing HEK293T cells were subjected to HS, followed by recovery in the presence or absence of cycloheximide (CHX). GFP fluorescence acquisition settings were identical in all images except for the bottom image were the GFP channel image +HS +REC +CHX was duplicated and brightness and contrast were enhanced (B/C enhanced). (**G**) NLS-LG level and specific luminescence activity in the indicated conditions. Data are expressed as % of control prior to heat stress (mean + SD, n = 4). Nuclei are marked with a dashed white line. Representative images of at least 3 biological repeats are shown. Scale bars (B, D) 1 µm, (E, F) 10 µm.
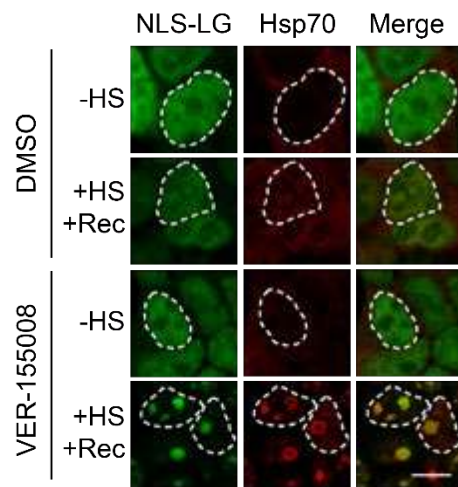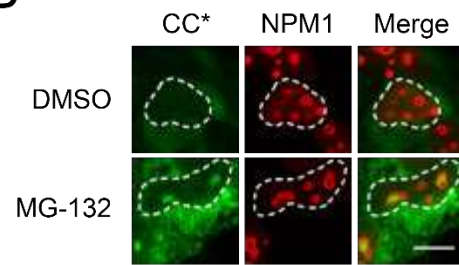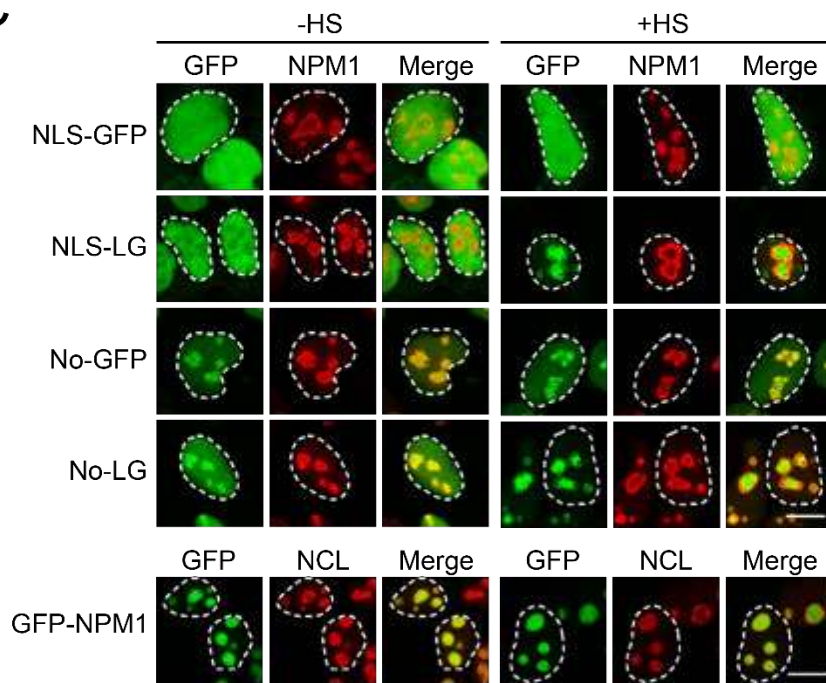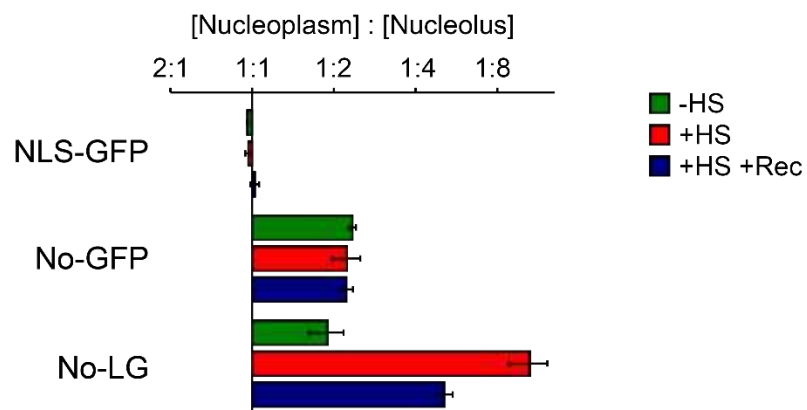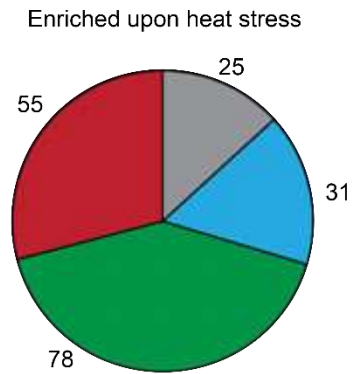
Fig. S2

Properties of nuclear and nucleolar proteins in control conditions and upon heat stress. (**A**) Repartitioning of NLS-LG from the nucleolus during recovery from stress is Hsp70-dependent. HEK293T cells expressing NLS-LG were maintained at 37 °C (-HS) or subjected to heat stress, followed by recovery (+HS +Rec) in the presence or absence of the Hsp70 inhibitor VER-155008 (*32*). Cells were immunostained for Hsp70 and NLS-LG visualized by GFP fluorescence. (**B**) Accumulation of the cytosolic misfolded protein CPY*-mCherry (CC*) in the nucleolus upon proteasome inhibition. HEK293T cells transiently expressing CC* were grown at 37 °C and treated with DMSO or MG132 for 12 h. CC* was visualized by mCherry fluorescence (shown in green) and cells were immunostained for endogenous NPM1. (**C**) Cellular localization of NLS-LG, No-LG, NLS-GFP, No-GFP and GFP-NPM1 proteins in control conditions and upon heat stress in HEK293T. Cells were immunostained for endogenous NPM1 or nucleolin (NCL) to highlight nucleoli. (**D**) Partition coefficient between nucleoplasm and nucleoli of the indicated constructs transfected into HEK293T cells subjected to +HS, +HS +Rec or left at 37 °C (-HS). Endogenous NPM1 was used to detect nucleoli. The partition coefficient [Nucleoplasm] : [Nucleolus] is plotted using a logarithmic scale and is depicted as mean ± SD of 3 biological repeats representing 60-102 cells per condition. Nuclei are marked with a white dashed line. Representative images of at least 3 biological repeats are shown. Scale bars 10 μm.
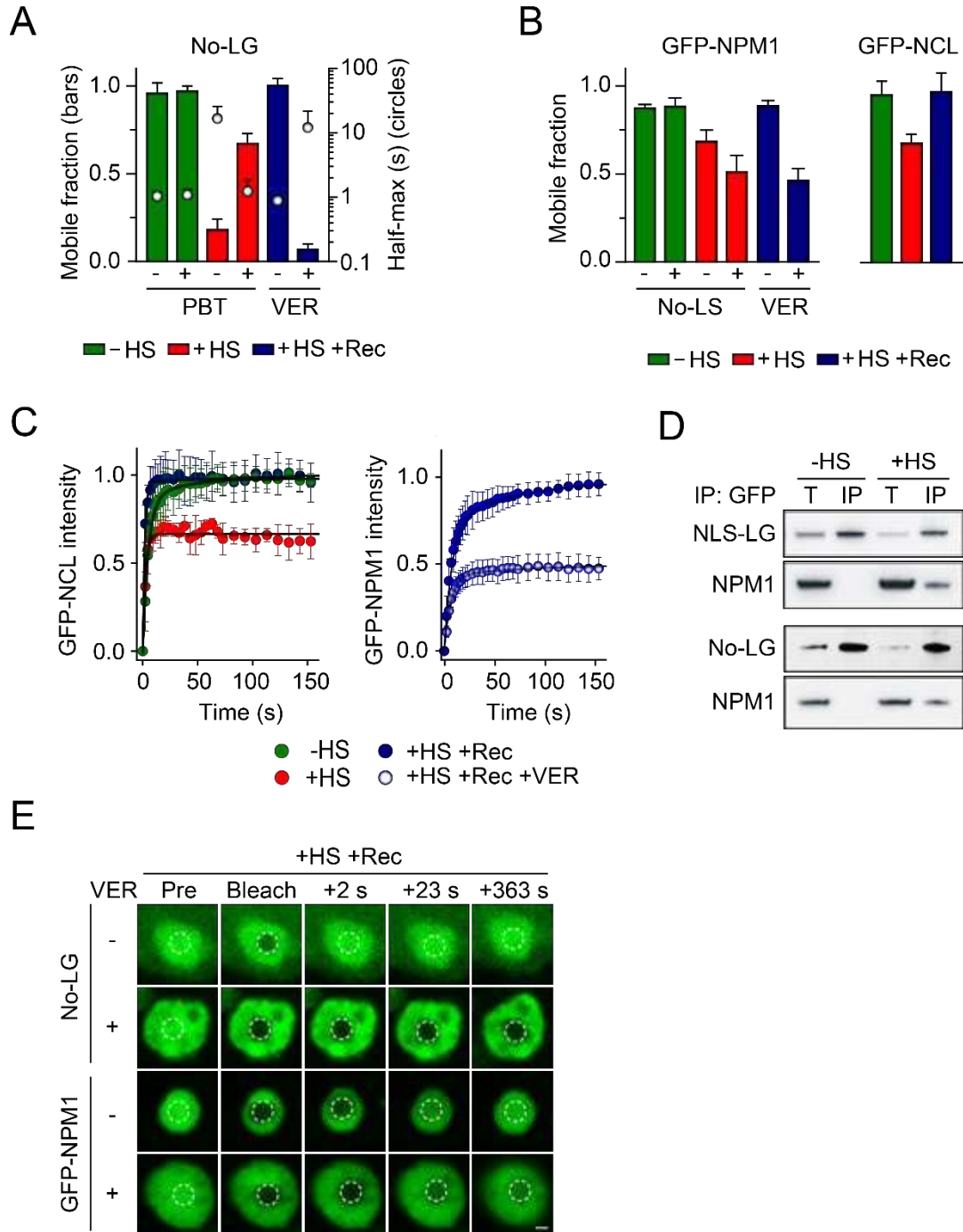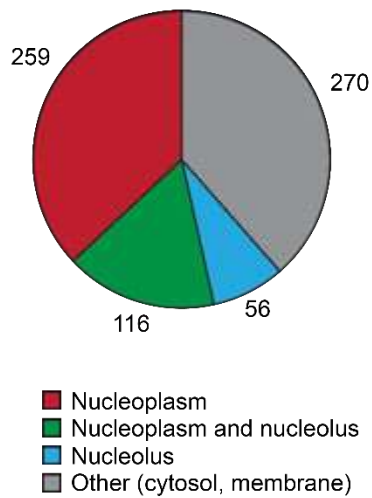
Fig. S3

Mobility of proteins in the nucleolus in control conditions and during heat stress.

(**A**) and (**B**) Quantification of mobile fractions of No-LG (A), GFP-NPM1 and GFP-NCL

(B) from FRAP experiments in Fig. 1E and F and fig. S3C. Graphs display the mobile

fraction on the left axis and the half-time of recovery (A only) on the right axis. Means +

SD of at least 3 biological repeats are shown. (**C**) Left graph; FRAP curves of GFP-NCL

transfected into HEK293T cells and subjected to FRAP as GFP-NPM1 (Fig. 1F). The

graph displays normalized FRAP curves as mean ± SD (n ≥ 3, representing at least 9

cells) with double exponential fits. Right graph; recovery of GFP-NPM1 mobility after

HS requires functional Hsp70. Cells expressing GFP-NPM1 were subjected to 2 h HS

and 1 h recovery at 37 °C, followed by FRAP. Hsp70 inhibition during recovery was

performed by adding VER-155008 before shifting cells to 37 °C. CHX was always

present during recovery. Curves are given as mean ± SD (n ≥ 4, representing at least 12

cells). (**D**) NPM1 binds to NLS-LG and No-LG upon heat stress. NLS-LG (top panels) or

No-LG (bottom panels) expressing cells were heat stressed or maintained at 37 °C before

immunoprecipitation of NLS-LG or No-LG. Representative immunoblots of NPM1 and

GFP are shown (3 independent experiments). T, input fraction; IP, eluated

immunoprecipitate. 1.0% of the input and 14.3% of the eluate were analyzed.

(**E**) Dependence on Hsp70 activity of No-LG and GFP-NPM1 mobility during recovery

from heat stress. Selected FRAP time point images from the recovery experiments

displayed in Fig. 1E (No-LG; right panel) and fig. S3C (GFP-NPM1; right panel). The

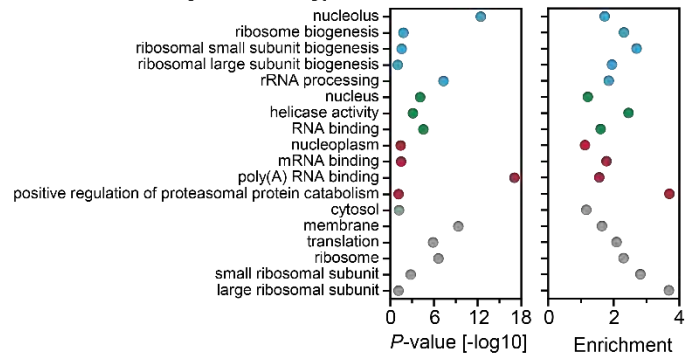bleached area is marked with a dashed circle. Scale bar 1 μm.
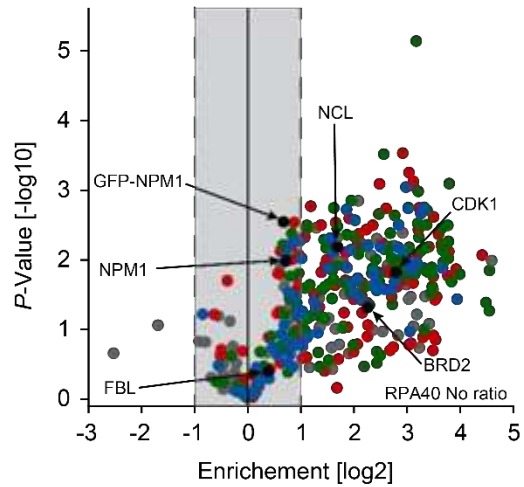
A

Enriched upon heat stress

55, 25, 31, 78

Background/
heat stress independent

259, 270, 116, 56

- Nucleoplasm
- Nucleoplasm and nucleolus
- Nucleolus
- Other (cytosol, membrane)

B

Enriched gene ontology terms

nucleolus
ribosome biogenesis
ribosomal small subunit biogenesis
ribosomal large subunit biogenesis
rRNA processing
nucleus
helicase activity
RNA binding
nucleoplasm
mRNA binding
poly(A) RNA binding
positive regulation of proteasomal protein catabolism
cytosol
membrane
translation
ribosome
small ribosomal subunit
large ribosomal subunit

P-value [-log10]   Enrichment

Gene ontology associated with:
- Nucleolus
- Nucleoplasm and nucleolus
- Nucleoplasm
- Other (cytosol, membrane)

C

P-Value [-log10] vs Enrichement [log2]

NCL
GFP-NPM1
NPM1
CDK1
BRD2
FBL
RPA40 No ratio

D

P-value 2.2*10^-3 — Longest disodered sequence

P-value 1.5*10^-4 — Longest LC sequence

P-value 5.5*10^-7 — Frequency of disordered residues

P-value 8.0*10^-9 — Frequency of LC residues

- Proteome
- Associated proteins enriched upon HS

Fig. S4

GFP-NPM1 associates with endogenous proteins upon heat stress. (**A**) Subcellular localization of GFP-NPM1 associated (upper chart) and non-associated proteins (bottom chart) upon HS. Localization of proteins is based on gene ontology (GO) cell compartment analysis. Proteins were classified as nucleoplasmic (red), nucleoplasmic and nucleolar (green), nucleolar (blue) or other (grey), mostly being cytosolic or from membranes (see Table S1 and Methods). (**B**) GO analysis of GFP-NPM1 associated proteins upon HS. Enriched GO terms were trimmed to avoid redundancy. Fisher Exact *P*-values and enrichment of the terms over all identified proteins are shown. GO terms were associated with a cellular compartment and color coded as in (A). (**C**) Volcano plot representation of proteins identified in at least 3 repeats in the GFP-NPM1 pull down upon +HS and -HS. Protein localization is color coded as in (A). Proteins mentioned in the manuscript are indicated. (**D**) Distribution of longest disordered amino acid sequences and low complexity sequences, as well as frequency of residues in disordered regions and in low complexity regions in GFP-NPM1 associated proteins upon heat stress compared to the human proteome. DISOPRED and SEG program were used to assess disordered and low complexity regions, respectively. Dashed horizontal lines indicate the median, box limits indicate 25th/75th, and whisker caps 5th/95th percentiles, respectively. *P*-values are calculated from a two-sided Mann-Whitney U test.
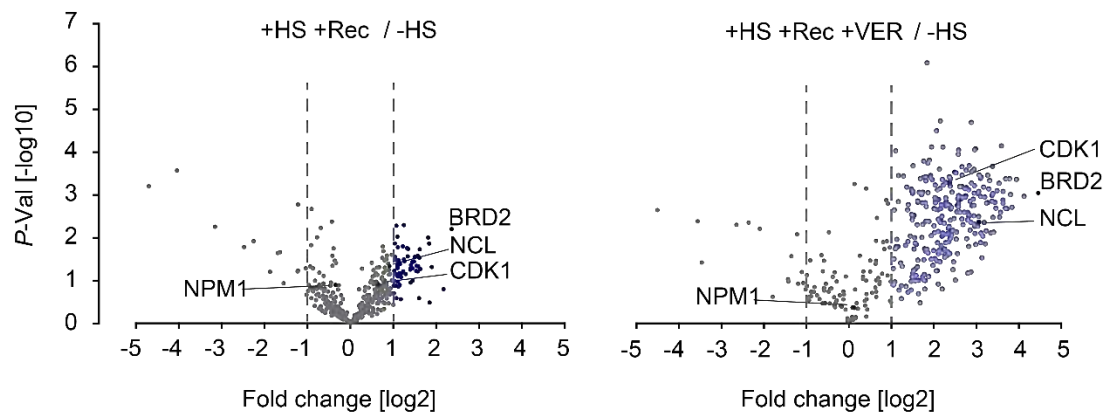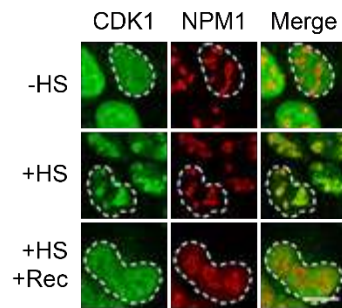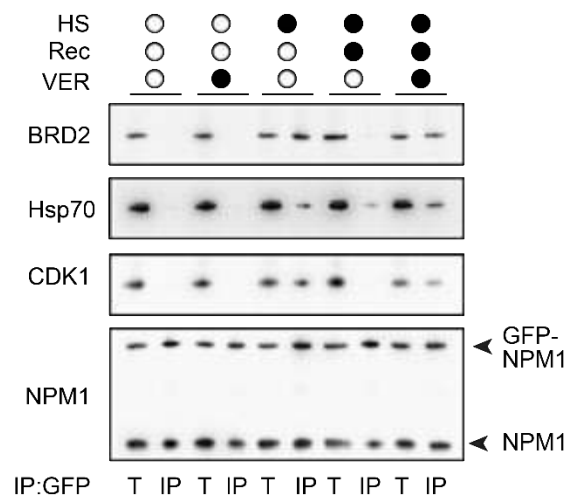
Fig. S5

Release of GFP-NPM1 associated endogenous proteins during recovery is Hsp70 dependent. (**A**) Volcano plot representation of proteins identified in at least 3 repeats in the GFP-NPM1 SILAC pulldown comparing +HS +Rec and –HS (left plot) and +HS +Rec +VER and –HS (right plot). SILAC labeled HEK293T cells expressing GFP-NPM1 were subjected to heat stress at 43 °C for 2 h and followed by recovery at 37 °C for 2 h in presence (+HS +Rec +VER) or absence (+HS +Rec) of the Hsp70 inhibitor VER-155008 during the recovery. Control cells were maintained at 37 °C (-HS). Fold change as well as the associated *P*-Value of the t-test are shown. Proteins mentioned in the text are indicated. (**B**) CDK1 transiently accumulated in the nucleolus upon heat stress. HEK293T cells were subjected to heat stress at 43 °C for 2 h (+HS), followed by recovery at 37 °C for 2 h (+HS +Rec). Control cells were maintained at 37 °C (-HS). Cells were immunostained for endogenous NPM1 and for cyclin-dependent kinase 1 (CDK1). Nuclei are marked with a white dashed circle. Representative images of 3 biological repeats are shown. Scale bar 10 μm. (**C**) HEK293T cells expressing GFP-NPM1 were treated as indicated. GFP-NPM1 was immunoprecipitated and total fractions as well as eluates were analyzed by immunoblotting against indicated proteins. T, input fraction; IP, eluted immunoprecipitate. 1.0% of the input and 14.3% of the eluate were analyzed.
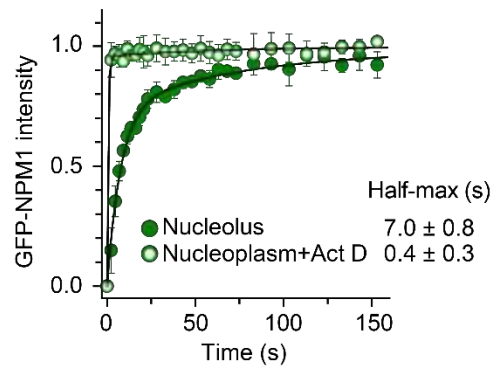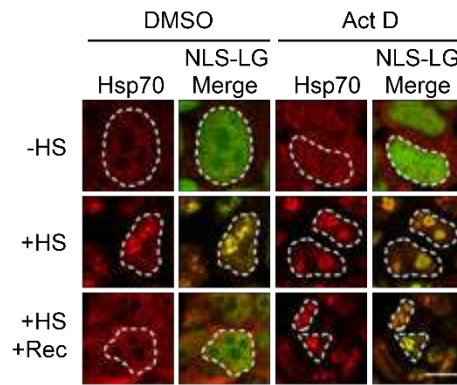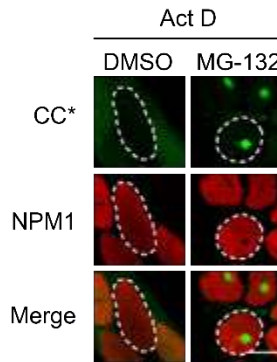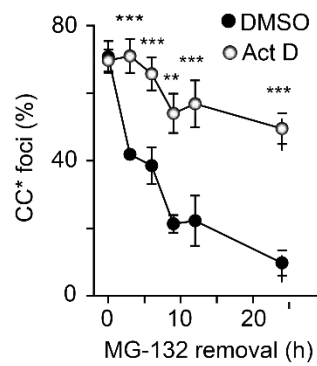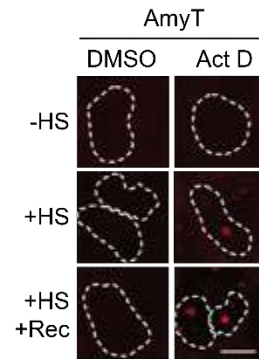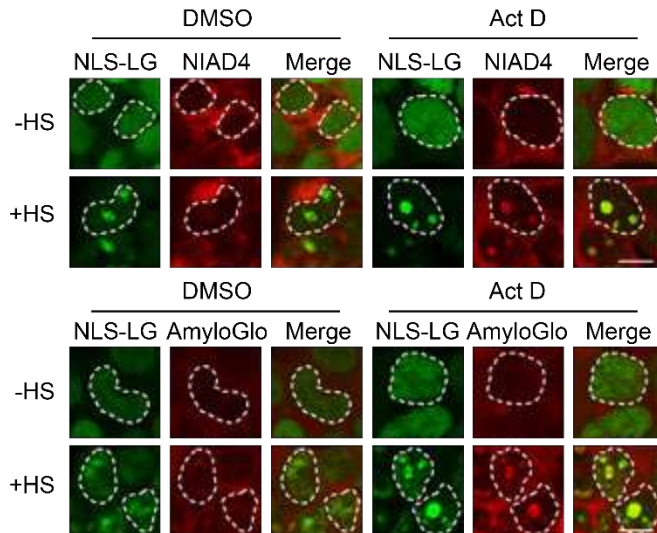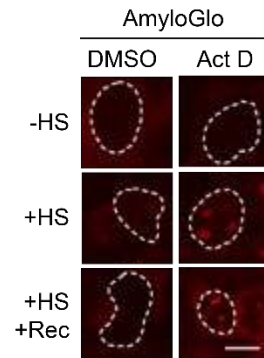
Fig. S6

The GC phase of the nucleolus stabilizes misfolded proteins during heat stress in a state competent for refolding or degradation upon recovery. (**A**) Actinomycin D (Act D) treatment disturbs the liquid-phase behavior of NPM1. FRAP analysis of nucleolar GFP-NPM1 and of nucleoplasmic GFP-NPM1 upon Act D treatment (mean ± SD; n ≥ 3; 9 cells per condition). FRAP data of nucleolar GFP-NPM1 are also shown in Fig. 1F. (**B**) Nucleoplasmic aggregates of NLS-LG formed upon heat stress in Act D treated cells sequester Hsp70. HEK293T cells expressing NLS-LG were treated as in Fig. 3A and stained for Hsp70. (**C**) CC* forms nucleoplasmic foci upon proteasome inhibition in Act D treated cells. HEK293T cells expressing CC* were treated with Act D and either DMSO or MG-132. Cells were immunostained for endogenous NPM1, and CC* was visualized by mCherry fluorescence (shown in green). (**D**) Aggregation in the nucleoplasm delays CC* degradation upon removal of proteasome inhibitor. HEK293T cells expressing CC* were treated as in (C) and recovery was monitored over 24 h after removal of MG-132 and Act D. Cells with visible nuclear CC* foci were counted during recovery and expressed as percentage of total. Data are displayed as mean ± SD; 196 to 410 cells were counted per time point and condition across 3 biological repeats. *P*-values from two-sided *t*-tests are shown. (**E**, **F** and **G**) Act D treated cells form foci in the nucleoplasm upon heat stress, that can be stained with amyloid-specific dyes, which persist upon recovery. NLS-LG expressing cells (E) or non-transfected HEK293T (F, G) were treated as in Fig. 3D. Cells were stained with NIAD4 (E), AmyloGlo (E, G) or AmyT (F). Nuclei are marked with a white dashed line. Representative images are shown. Scale bars 10 μm.
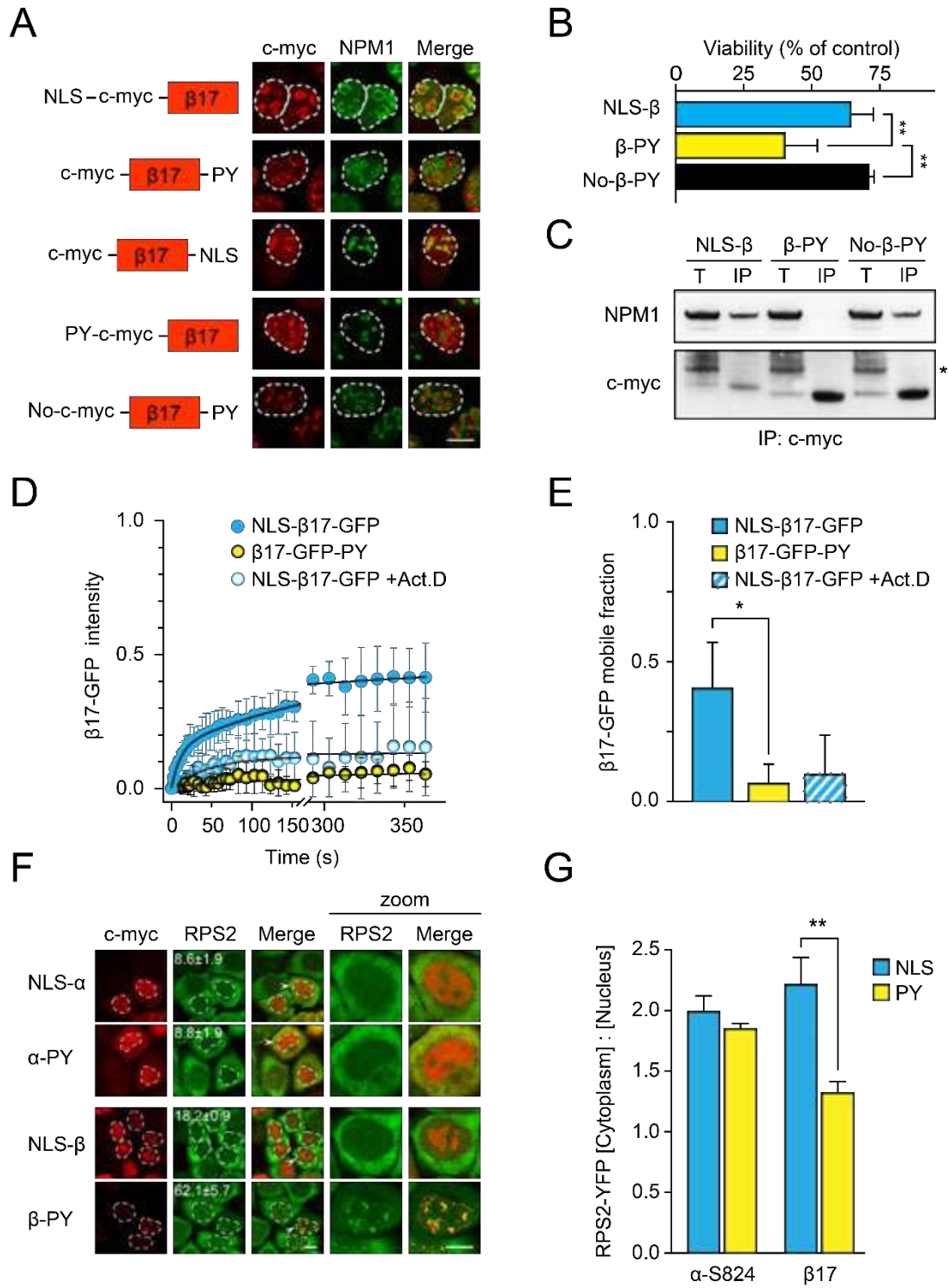
Fig. S7

The nucleolar environment prevents toxic protein aggregation. (**A**) Schematic

representation of the β17 protein constructs used in this study and their localization.

Immunostaining was performed against c-myc (β17) and NPM1. (**B**) Re-routing of β-PY

to the nucleolus (No-β-PY) rescued cellular viability. Data for NLS-β and β-PY are also

shown in Fig. 4C. (**C**) HEK293T cells were transfected with the indicated β17 constructs.

After immunoprecipitation, β17 and NPM1 were analyzed. T, input fraction; IP, eluted

immunoprecipitate. 1.0% of the input and 14.3% of the eluate were analyzed; *, non-

specific band. Representative immunoblots of 3 biological repeats are shown. (**D**) β17

foci formed in the nucleoplasm of Act D treated cells are immobile. FRAP analysis of

NLS-β17-GFP and β17-GFP-PY expressed in HEK293T cells. Where indicated, NLS-

β17-GFP expressing cells were treated with Act D for 4 h before acquisition. Curves are

given as mean ± SD (n=3; 13-17 cells per condition). (**E**) Mobile fractions of β17

proteins from FRAP measurements described in (D) expressed as mean + SD; *P*-value of

two-sided t-test is indicated. (**F**) Export of ribosomal particles from the nucleus is not

affected by β17 proteins in the nucleolus. HeLa Tet-On RPS2-YFP cells were transfected

with the indicated constructs and immunostained against c-myc. Zoomed images show

cells indicated by arrowheads. Numbers represent the percentage of transfected cells with

an abnormal pattern of cellular RPS2-YFP distribution (mean ± SD, n=3, at least 150

cells per conditions) (**G**) Partition coefficient of RPS2-YFP between the cytoplasm and

nucleus of transfected cells from (F) expressed as mean + SD. *P*-value of two-sided t-test

is shown. Nuclei are highlighted with a white dashed line. Representative images are
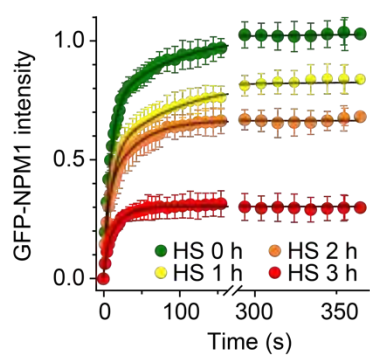
shown. Scale bars, 10 μm.
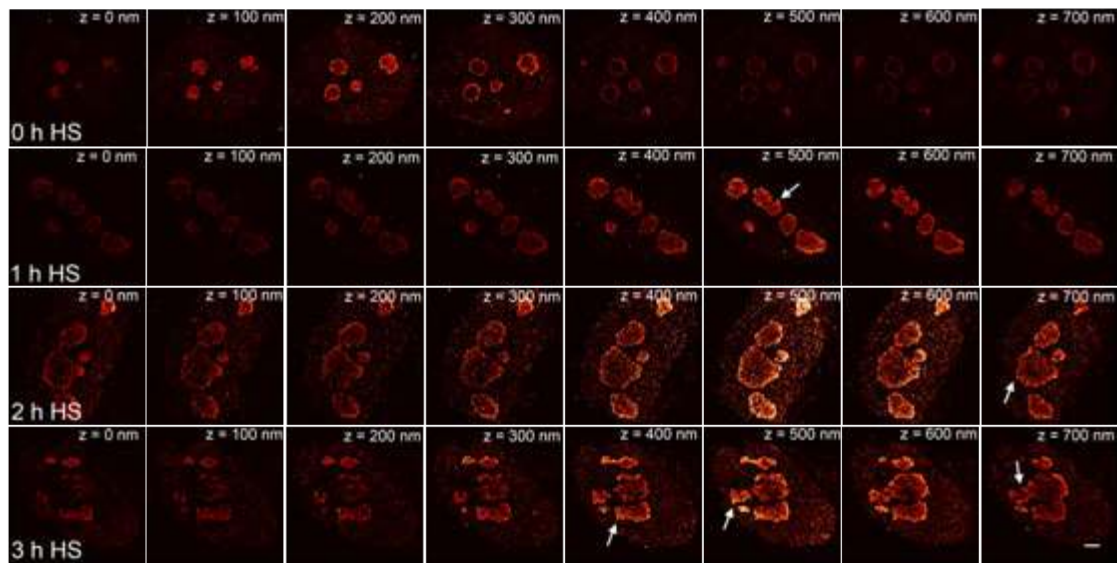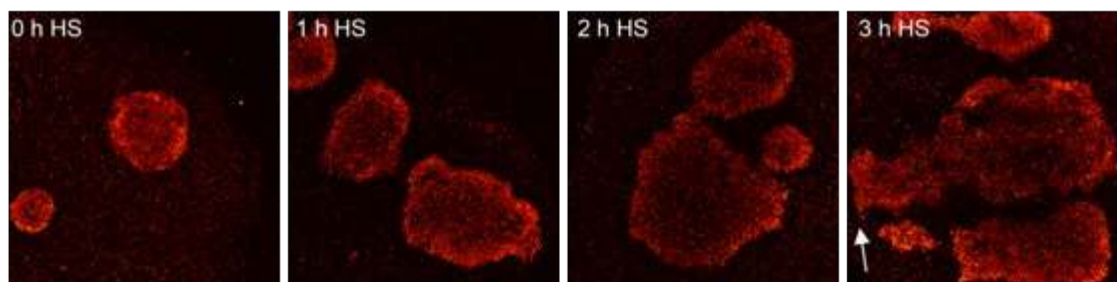
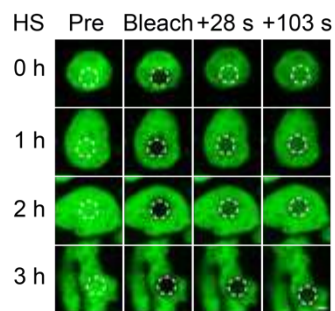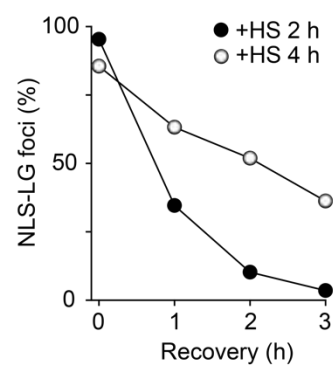**Fig. S8**

Nucleolar aging upon prolonged proteotoxic stress. (**A**) HeLa cells were subjected to
43 °C for 1, 2 or 3 h or maintained at 37 °C before analysis by DNA PAINT and super-
resolution imaging of endogenous NPM1. Z-stack series are shown. Note the loss of
nucleolar roundness with time under heat stress and the appearance of sharp edges
(arrows) inconsistent with a liquid droplet. (**B**) Zoomed images of the z-series shown in
(A) from -HS to 3 h HS (left to right images) as a z-projection. (**C**) Time dependent loss
of NPM1 mobility during prolonged heat stress. HeLa cells transfected with GFP-NPM1
were subjected to FRAP analysis after 0, 1, 2 or 3 h of HS. Fluorescence recovery of the
bleached region (within the nucleolus) was monitored for 350 s. Normalized, corrected
and average FRAP curves are shown as well as associated exponential fits. The curves
are shown as mean ± SD. The computed mobile fractions are shown in Fig. 5B.
(**D**) Images of selected time points from the GFP-NPM1 FRAP experiment described in
(C) and Fig. 5B. Images show a single nucleolus. The bleached area is indicated with a
dashed white circle. (**E**) HEK293T cells expressing NLS-LG were subjected to 2 h or 4 h
of heat stress before placing them at 37 °C for recovery (0 to 3 h). After fixation, cells
with nucleolar NLS-LG foci were counted and expressed as percentage of total number
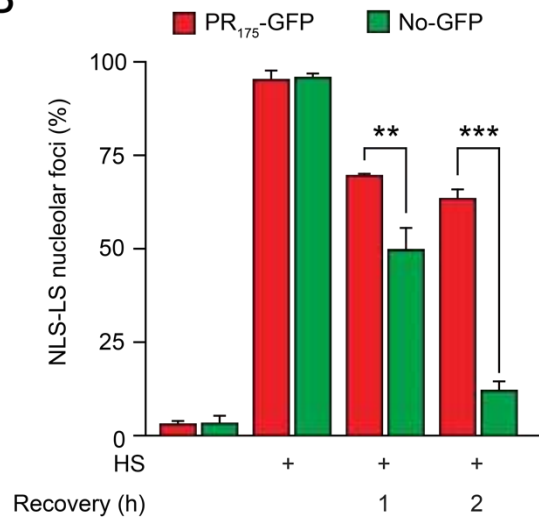of cells. 125-252 cells were analyzed per condition. Scale bars, 1 μm.
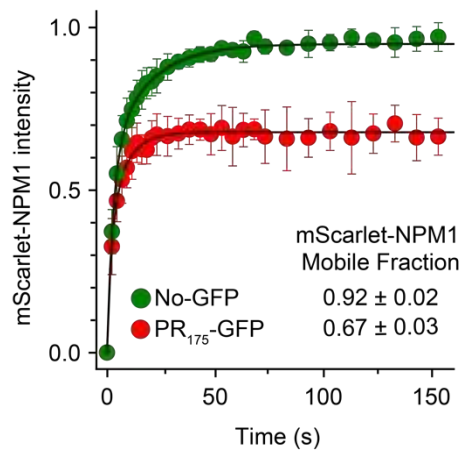
Fig. S9

Expression of arginine containing dipeptide repeat protein perturbs nucleolar function. (**A**) FRAP analysis of mScarlet-NPM1 in HEK293T cells co-transfected with either PR_{175}-GFP or the nucleolar control protein No-GFP. After photobleaching a region inside the nucleolus containing both constructs (mScarlet-NPM1 and No-GFP or mScarlet-NPM1 and PR_{175}-GFP) fluorescence recovery of mScarlet-NPM1 was monitored. Normalized and averaged fluorescence recovery curves with exponential fits, corrected for photobleaching are shown for mScarlet-NPM1 in presence of No-GFP (green) or PR_{175}-GFP (red). The mobile fraction of mScarlet-NPM1 in presence of either No-GFP or PR_{175}-GFP was extracted from the exponential curve fits. The curves are shown as mean ± SD from 4-5 biological repeats representing 20-24 cells per condition. (**B**) Dipeptide repeat protein slows repartitioning of NLS-LS from the nucleolus during recovery from stress. Quantification of the experiment described in Fig. 5D. Cells with nucleolar NLS-LS in presence of either PR_{175}-GFP or No-GFP were quantified. Data are plotted as percentage of transfected cells. Means + SD from 3 biologicals repeats are shown and represent 87 − 140 cells analyzed per condition and construct. *P*-Value of two-sided t-test is displayed.

Caption for Table S1

Proteins associated with GFP-NPM1 upon heat stress. List of proteins associated with GFP-NPM1 in HEK293T cells exposed to heat stress (2 h at 43 °C) (+HS) determined by SILAC. Cells not exposed to heat stress (-HS) served as control. SILAC ratios of +HS/-HS of 4 independent experiments are shown. Associated proteins (ratio > 2 in at least 3 experiments, see Methods) are colored according to protein localization as in fig. S4A; nucleoplasm (red); nucleoplasm and nucleolus (green); nucleolus (blue); other (grey). Non associated proteins are uncolored. Intensity-based absolute quantification (iBAQ) values reflect measured molar protein amounts.

Caption for Table S2

Proteins associated with GFP-NPM1 during recovery. List of proteins associated with GFP-NPM1 in HEK293T cells exposed to heat stress (2 h at 43 °C) followed by recovery (2h at 37 °C) (+HS +Rec) determined by SILAC. Cells not exposed to heat stress (-HS) served as control. SILAC ratios of +HS +Rec/-HS of 4 independent experiments are shown. Associated proteins (ratio > 2 in at least 3 experiments, see Methods) are shown. Intensity-based absolute quantification (iBAQ) values reflect measured molar protein amounts.

Caption for Table S3

Proteins associated with GFP-NPM1 during recovery and Hsp70 inhibition. List of proteins associated with GFP-NPM1 in HEK293T cells exposed to heat stress (2 h at 43 °C) followed by recovery (2h at 37 °C) and treatment with the Hsp70 inhibitor VER-155008 (+HS +Rec +VER) determined by SILAC. Cells not exposed to heat stress (-HS) served as control. SILAC ratios of +HS +Rec +VER/-HS of 4 independent experiments

are shown. Associated proteins (ratio > 2 in at least 3 experiments, see Methods) are shown. Intensity-based absolute quantification (iBAQ) values reflect measured molar protein amounts.